JNC TN9400 2001-096

Interpretation of the CABRI-RAFT LTX Test up to Pin Failure based on Detailed Data Evaluation and PAPAS-2S Code Analysis

September 2001

O-arai Engineering Center
Japan Nuclear Cycle Development Institute

Ⓢ

Interpretation of the CABRI-RAFT LTX Test up to Pin Failure based on Detailed Data Evaluation and PAPAS-2S Code Analysis

Yoshitaka FUKANO※ and Ikken SATO※

Abstract

The CABRI-RAFT LTX test aims at a study on the fuel-pin-failure mechanism, in-pin fuel motion and post-failure fuel relocation with an annular fuel pin which was pre-irradiated up to peak burn-up of 6.4 at.%. The transient test conditions similar to those of the LT4 test were selected in the LTX test using the same type of fuel pin, allowing an effective direct comparison between the two tests. In contrast to the LT4 test which showed a large PCMI-mitigation potential of the annular fuel-pin design, early pin failure occurred in the LTX test when fuel does not seem to have molten.

In order to clarify the fuel pin failure mechanism, interpretation of the LTX test up to pin failure is performed in this study, through an experimental data evaluation and a PAPAS-2S-code analysis. The PAPAS-2S code simulates reasonably the fuel thermal conditions such as transient fuel-pin heat-up and fuel melting. The present detailed data evaluation shows that the earlier cladding failure compared with the LT4 test is mainly attributed to the local cladding heat-up. Under the high-temperature condition, plenum gas pressure has a certain potential to explain the observed failure. Fuel swelling-induced PCMI does not seem significant in the LTX test and it may have contributed to the early pin failure only to a limited extent, if any.

※Nuclear System Safety Research Group, Advanced Technology Division, O-arai Engineering Center

試験データの詳細分析及びPAPAS-2Sコード解析による CABRI-RAFT計画LTX試験の燃料破損挙動の解釈 (研究報告書)

深野　義隆※　　佐藤　一憲※

要旨

CABRI-RAFT計画LTX試験はピーク燃焼度6.4%の中空燃料を用いて、燃料ピンの破損メカニズム、ピン内燃料移動、及び破損後燃料移動挙動を解明することを目的としている。過渡の試験条件は、同様の燃料ピンを用いたLT4試験と同様の試験条件としており、両試験は効果的な比較が可能である。同種の燃料ピンの高いPCMI緩和ポテンシャルを示したLT4試験とは対照的に、LTX試験では、燃料溶融に至る前の早期の燃料ピン破損が生じた。

本研究では、燃料ピンの破損メカニズムを明らかにするために、試験データの評価、及びPAPAS-2Sコードを用いた解析を通じ、LTX試験の燃料ピンの破損に至るまでの解釈を行った。PAPAS-2Sコードによる解析結果は燃料溶融等の熱的条件を十分に模擬している。また、詳細な試験データ評価により、LT4試験に比べて早期に発生した燃料ピン破損は基本的には被覆管の局所的な高温化によることが分かった。このような高温条件では、プレナムガス程度の機械的負荷でも破損を説明し得る。一方、過渡時の燃料スウェリングによるPCMI負荷は顕著なものではなく、例え観測された早期ピン破損に寄与していたとしても、その効果は限定的なものであると考えられる。

※大洗工学センター　要素技術開発部　リスク評価研究グループ

Contents

List of Table and Figures

1. Introduction

The LTX test in the CABRI-RAFT program was performed on March 16th, 2000 with the SCARABIX-CABRI type annular fuel pin which was pre-irradiated in the PHENIX reactor up to peak burn-up of ~6.4 at.%.

The main objectives of this test are:

- to study a fuel pin failure mechanism and failure condition with the annular fuel under the TUCOP (Transient Undercooling Overpower) condition,
- to study possible in-pin fuel motion, especially the fuel squirting before cladding failure toward the gas plena through the central holes connecting the fissile region and the gas plena, and
- to study post-failure fuel dispersal and relocation in the coolant channel.

In order to fulfill these objectives, the following modifications were made on the test fuel pin:

- the original fertile pellets without central hole were replaced with annular insulators in order to enhance the in-pin molten fuel motion into the plena through the fuel central hole, and
- a new device was installed just above the TFC (Top of Fissile Column) so as to detect the arrival of the squirted fuel.

The transient test conditions adopted in the LTX test were similar to those of the LT4 test[1] in which the same type of fuel pin had been used without above-mentioned modification.

While the LT4 test showed a high potential to mitigate PCMI (Pellet-Cladding Mechanical Interaction) with the late pin failure at 621 ms after TOP (Transient Overpower) onset, a rather early pin failure at 460 ms after TOP onset took place in the LTX test.

In this study, interpretation of the LTX test up to pin failure is performed through a detailed data evaluation and a PAPAS-2S code analysis in order to clarify the fuel pin failure mechanism and the fuel condition at the observed failure.

2. Overview of the test

2-1. Test conditions

In the LTX test, TOP was triggered during LOF (Loss of Flow) before coolant boiling, under a transient condition similar to that of the LT4 test and using the same SCARABIX-CABRI type fuel pin. Table 1 shows comparison of the test conditions and main test results between these tests. Pin failure took place both in these TUCOP tests at quite different timing during TOP.

In the LTX test, steady-state linear-power rating in CABRI was 508 W/cm, which was almost the same as the LT4 value (512 W/cm). TOP was automatically triggered at 18.457 s after the LOF onset, when the average TFC coolant temperature reached 893 °C. The power history is also the same as that of the LT4 test as presented in Figure 1.

2-2. Test results

During LOF, fissile-fuel elongation of 2 (±2) mm was observed by the neutron hodoscope up to the TOP triggering, while that in the LT4 test was 3 (± 2) mm. TCs in the coolant channel caught considerable azimuthal temperature variation (19.0 K at TFC) corresponding to pin bending during the steady state. The temperature variation became more than twice (39.7 K at TFC) by the end of LOF and it increased further during TOP. Although the azimuthal temperature variation during the steady state was comparable to that in the LT4, it became larger during LOF than that in the LT4 test (33.9K at TFC). Therefore, the pin bending in the LTX test is considered to have been larger than the LT4 test. Although no meaningful pin bending during LOF was detected by the hodoscope in the LT4 test, it should be noted that the direction of the observed initial temperature gradient was almost parallel to the hodoscope viewing direction. Thus the probable bending would not be detected by the hodoscope anyway.

The structured TOP with its main-pulse peak of 45.55 Po was applied to this test and it resulted in energy injection of 1.11 kJ/g before SCRAM. Some events detected by various measurement means are presented in Figure 2. At 407 ms, gradual sodium flow divergence started and this seems to have been an onset of local sodium boiling. At 430 ms after TOP onset, sodium temperature

at 60cm/BFC (cm from Bottom of Fissile Column) exceeded the saturation temperature of 975 °C at the hottest azimuth.

In contrast to the LT4 test, early pin failure occurred in the LTX test at 460 ms after TOP onset, when fuel does not seem to have molten. After the probable cladding failure at 460 ms, a rapid coolant flow rate change occurred, which is likely to have been gas release from the pin.

A rapid change of displace-transducer(DT) signal corresponding to the pin-top displacement was observed at 526 ms after TOP onset. The hodoscope caught fuel-signal increase just above TFC after ～530 ms. These events indicate sudden upward motion of the upper pin segment.

3. Interpretation through data evaluation and code analysis

3-1. Analytical condition and assumptions

The PAPAS-2S input data set for the LTX test is prepared based on that for the LT4 test. The transient power history, the axial power profile and the LOF curve are well fitted to the experimental data of the LTX test as shown in Figures 3 to 5.

In the LT4 test analysis, pin-internal volumes such as fuel-to-cladding gap and macroscopic cracks available for mitigating PCMI were regarded as uncertain parameters. Through a parametric study, it was concluded that a certain fraction of such volumes was available to mitigate the PCMI. In the LT4 reference case which reasonably simulated the observed result, 100% availability of the gap and 50% availability of the cracks were adopted. Quantitative information on such volumes are available from the radial cuts on the sibling pin as presented in Figure 6.

In the present study for the LTX test, 0%, 50% and 100% availability of macroscopic-crack volume are adopted for survey with the 100% gap-volume availability.

From the sublimation measurement, amount of local gas retention is available at many axial positions of the SCARABIX-CABRI type fuel. However, the axial gas retention profile seems affected considerably by the local chamfer effect. Therefore, in the present PAPAS-2S study, global gas retention within the fuel is defined first based on the pin-piercing data. This global retention is distributed within the fuel using axial and radial gas-retention profiles provided by the SAS4A (REF96R1.FZK version) calculation. The axial and radial gas profiles used in the present PAPAS-2S study are presented in Figures 7 and 8. An intergranular-gas fraction is assumed to be 50% based on the sublimation and EPMA data.

Before the transient calculation, a steady-state coolant thermal condition is checked. The calculated coolant temperature profile during the steady state is presented in Figure 9 together with the TC data. Although the calculated temperature at the TFC is slightly lower than the average of the TC data at this axial level, the PAPAS-2S result is in reasonable agreement with the

experimental thermal condition during the steady state. Probable explanation for this slight difference at TFC is possible overestimation of heat loss to the surrounding Niobium-tube structure wall.

3-2. LOF behavior

The calculated coolant-temperature history at TFC during LOF agrees quite well with the average of experimental data as shown in Figure 10. The coolant temperature in the analysis stays lower initially but increases slightly faster in the early part of LOF compared with the TC data, leading to a better simulation of the average thermal condition in the later part of LOF. In the experiment, the coolant temperature rise was slightly delayed compared with the analysis and this could be explained by a possible reduction of gap conductance in the early part of LOF. As a result of the slight initial underestimation of the coolant temperature and the slight overestimation of temperature increase at the beginning of LOF, the coolant temperature at the TOP onset is almost equivalent to the average of the TC data.

Fuel and cladding elongation during the LOF up to the TOP onset calculated by PAPAS-2S is presented in Figure 11. The fuel elongation during LOF observed by the hodoscope is 2($\pm$2) mm, which is consistent with the calculated fuel elongation. Although the uncertainty in the hodoscope data is large, it is possible that the fuel elongation in the experiment was restricted due to the bending effect. Quantification of the cladding elongation during LOF was not possible by the DT device, which was designed specifically to detect the squirting event with reduced precision for the pin-top displacement. The calculated cladding elongation during LOF is 3.3 mm, which is similar to the observed fuel elongation.

3-3. TOP behavior

Coolant boiling was predicted at TFC at 421 ms after the TOP onset in the nominal PAPAS-2S calculation as depicted in Figure 12. On the other hand, coolant boiling took place near the 60 cm/BFC at 407 ms after the TOP onset in the LTX test while it initiated near the TFC in the LT4 test. The temperature reversal between 60 cm/BFC and TFC, present in LTX but not in LT4, is due

probably to the outstanding pin bending in the LTX test.

The cladding plastic strain calculated by PAPAS-2S during the PCMI phase with the different parameters for the mitigation-volume availability is presented in Figures 13 to 15. The calculated fuel volumetric swelling is presented in Figures 16 to 18. Although certain amount of fuel swelling is predicted, no plastic strain is calculated in the "100% gap and 100% crack-volume availability" and "100% gap and 50% crack-volume availability" cases at the observed cladding failure time of 460 ms after TOP onset. On the other hand, a maximum plastic deformation of 0.2%ΔD/D is calculated in the "100% gap and 0% crack-volume availability" case. Based on this result, it can be said that swelling-induced PCMI, if any, was not significant at the observed failure time. However, possibility of PCMI contribution to the early pin failure cannot be ruled out.

In the LTX test, rapid DT-signal increase was observed at 526 ms after TOP onset as presented in Figure 19. Figure 20 shows fuel melting boundary at the time of this DT event. Considerable fuel melting is calculated and the cavity pressure at this time is approximately 60 bar as presented in Figure 21. It should be noted that the cavity pressure rapidly increases after the initiation of fuel melting as the fuel melting extends.

A time integration of the coolant-flow-rate difference between outlet and inlet, from the time of pin failure to the time of DT event, is approximately 64 cm^3 in volume. If we assume that the ejected gas is responsible for this void-volume increse, and that the gas temperature and pressure in the coolant channel are 1000 °C and 2.5 bar, respectively, the amount of ejected gas is estimated to be 34 cm^3STP. On the other hand, the total plenum-gas volume obtained from the destructive examination for the SCARABIX-CABRI type pin is 348 cm^3STP. Therefore, the amount of ejected gas before the DT event is only ~10% of the initial amount. This means that plenum gas pressure decrease during this phase is very small. Since plenum gas pressure at the time of pin failure is estimated to be ~50 bar, which is the same value in the MF2 test where the same SCARABIX-CABRI type fuel pin was used, plenum gas pressure of approximately 45 bar still remained at the time of the DT event.

Because of no evidence of molten fuel penetration into the hollow insulator region through the central hole from the destructive examination, the DT

event and the subsequent hodoscope event are considered to have been caused by an upward motion of the pin upper part. However, no upward motion of the fissile bottom was detected by the hodoscope. Therefore, the observed displacement can only be explained by total cladding disintegration at some axial level separating the pin into upper and lower segments. This total cladding disintegration is likely to have taken place at 60cm/BFC where initial cladding failure took place and cladding heat-up was highest.

4. Discussion on the failure mechanism

Figure 22 shows the comparison of observed coolant-temperature evolution at TFC during LOF between the LTX and LT4 tests. The azimuthal coolant-temperature variation during LOF in the LTX test is larger than that in the LT4 test. This variation becomes larger during TOP as shown in Figure 23. Similarly, the azimuthal coolant-temperature variation at 60 cm/BFC in the LTX test is larger than that in the LT4 test as shown in Fig.24. Furthermore, the coolant temperature at the hottest azimuth during TOP at 60 cm/BFC is much higher than that at TFC as presented in Figure 25.

These pieces of information clearly show that there was an outstanding effect of pin bending in the LTX test, which brought specifically high cladding-temperature condition around the observed failure location.

If we use the temperature difference between coolant and cladding mid-wall at 60cm/BFC calculated in PAPAS-2S as presented in Figure 26, the expected cladding temperature at the hottest TC azimuth is 1050 ℃. Considering the fact that the TC location does not necessarily correspond to the very hottest spot, the local cladding temperature may have been higher than 1050 ℃.

Figure 27 shows the relation between calculated cladding temperature and cladding hoop stress corresponding to the plenum-gas pressure for the existing slow-TOP tests. UTS (Ultimate Tensile Strength) data taken from the cladding of the Viggen-4 fuel pin is also presented. The strain rate of 5.0x10-4(1/s) is well corresponding to the slow-TOP transient condition. This figure indicates that the plenum-gas pressure can be the main driving force for cladding failure during the slow TOP under a high cladding-temperature condition. The cladding hoop stress corresponding to the plenum-gas pressure of the SCARABIX-CABRI type pin is assumed to be about 33 MPa during the slow TOP condition realized in the MF2 test. In the PFR/TREAT CO5 test, similar hoop stress corresponding to the plenum gas pressure is expected and cladding failure took place in this test. Although various cladding materials were used in the in-pile tests presented in Fig.27, UTS at high-temperature condition tends to reduce its variation. Based on this understanding and the MF2 and CO5 results, the failure temperature under the slow TOP condition with the cladding hoop

stress of 33MPa is judged to be about 1000℃.

UTS data of the irradiated 15-15Ti taken from the Viggen-4 fuel pin are plotted against the strain rate in Fig.28. Although the UTS above 900℃ is not available, the estimated failure temperature for the slow TOP tests provides useful information. On the other hand, the cladding strain rate during the PCMI phase leading to the observed failure time in the PAPAS-2S analysis is about 0.025[1/s] (see Fig.15). Taking into account the estimation that local cladding temperature was about 1050℃ or higher, possible LTX-failure condition driven by swelling-induced PCMI is also plotted in this figure. On the other hand, if the driving pressure is only plenum-gas pressure, failure temperature is estimated to be in the rage of 1100～1200℃.

Therefore, it can be concluded that the plenum-gas pressure itself has a certain potential to explain the early LTX failure with possible local cladding heat-up above 1050℃. Contribution of fuel swelling-induced PCMI to the failure is also possible under the low cladding-strength condition. In any case, the early cladding failure took place under the very high cladding-temperature condition, in which driving pressure similar to the plenum-gas pressure or only slightly above it is sufficient to cause the failure.

5. Conclusions

Interpretation of the LTX test up to pin failure was performed through the detailed data evaluation and PAPAS-2S code analysis. The PAPAS-2S code simulated reasonably the fuel thermal condition such as fuel melting. Although the PCMI-induced cladding deformation in the analysis at the observed failure time was not significant, such PCMI contribution cannot be ruled out.

Based on the evaluation of cladding temperature and its mechanical property including estimation from the slow TOP tests, it is concluded that the early cladding failure in the LTX test took place under the very high cladding-temperature condition. With this temperature condition, driving pressure similar to the plenum-gas pressure or only slightly above it is sufficient to cause the failure.

The early pin failure in the LTX test is likely to be due to the local coolant boiling induced by the pin bending, which is specific to the CABRI single-pin condition. However, the post-failure behaviors, such as fission gas and molten fuel ejection into the coolant channel, fuel disintegration under the continued cladding heat-up and axial relocation, are quite representative for the case of early pin failure. It should be noted that another early pin failure was observed in the CABRI-FAST LT1 test[2] with a higher burn-up fuel (12 at.%), in which no bending comparable to the LTX test was observed. In the next step, therefore, we plan to evaluate the post-failure behavior in the LTX test to understand the consequence of the early pin failure together with the LT1 test result.

Acknowledgement

The authors express their great appreciation for Mr. Takuhiro CHUBACHI of CSK Inc., who helped the analytical works and preparation of the figures.

References

[1] Y. Onoda and I. Sato, "Interpretation of the CABRI LT4 test with SAS4A-code analysis," JNC TN9400 2001-047, March 2001

[2] I. Sato and Y. Onoda, "Interpretation of the CABRI LT1 test with SAS4A-code analysis," JNC TN9400 2001-048, March 2001

Table 1 Comparison of test condition and main test results between the LTX and LT4 tests

	LTX	LT4
Fuel Type	Scarabix-CABRI	Scarabix-CABRI
Fissile length (mm)	750	750
Pin diameter (mm)	8.5	8.5
Po (W/cm)	507	512
Na Temp. at BFC (℃)	400	401
Na Temp. at TFC (℃)	580	579
Energy at end of pre-pulse(480ms) (J/g)	499	499
Energy at 720ms (kJ/g)	1.10	1.10
Energy at 1.2s (kJ/g)	1.22	1.22
TOP Trigger (s after LOF onset)	18.457	18.651
TFC Na Temp. at TOP onset (℃)	893	897
Boiling onset (ms after TOP onset)	407	398
Pin failure (ms after TOP onset)	460	621

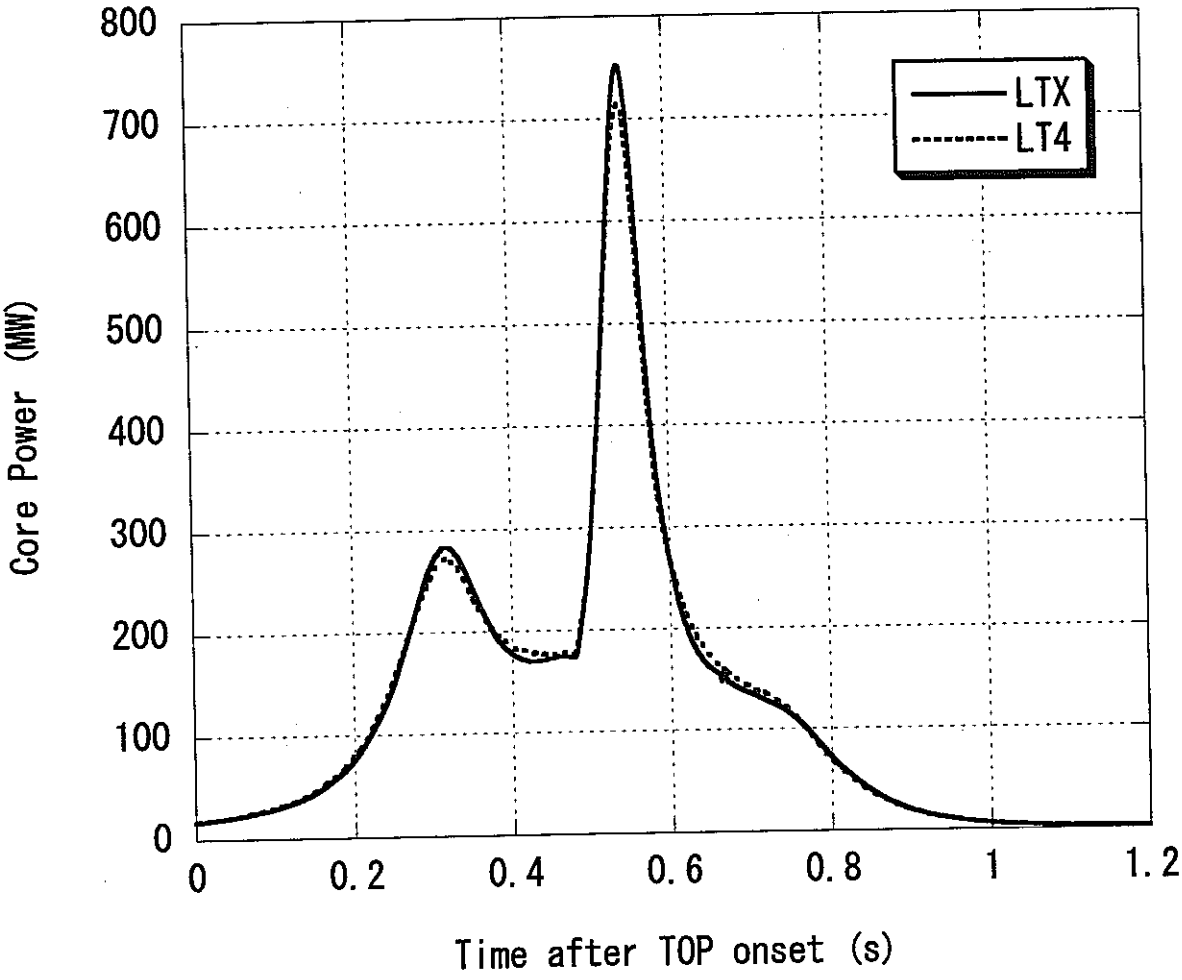

Figure 1 Comparison of power history during TOP between the LTX and LT4 tests

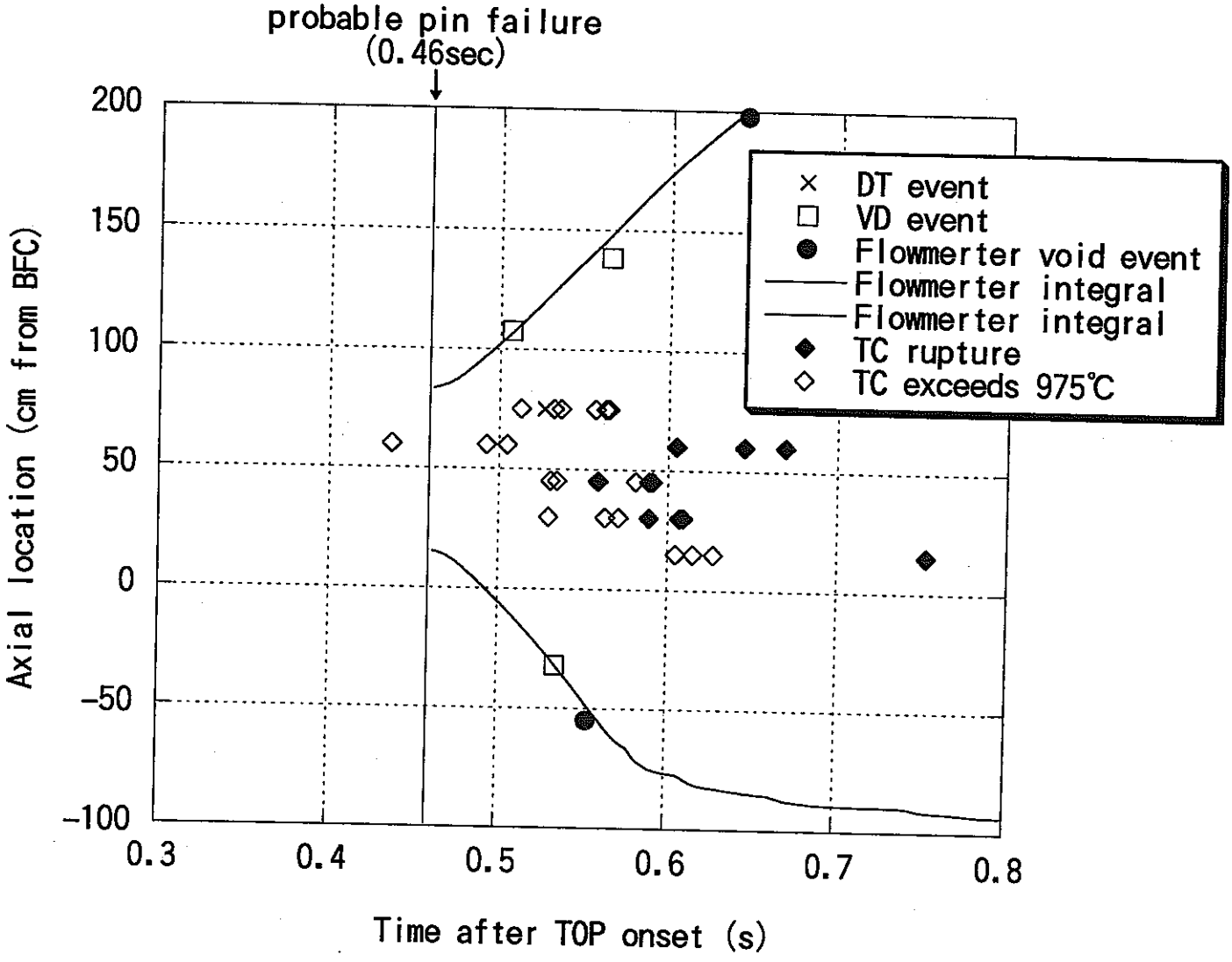

Figure 2 Main events observed during TOP in the LTX test

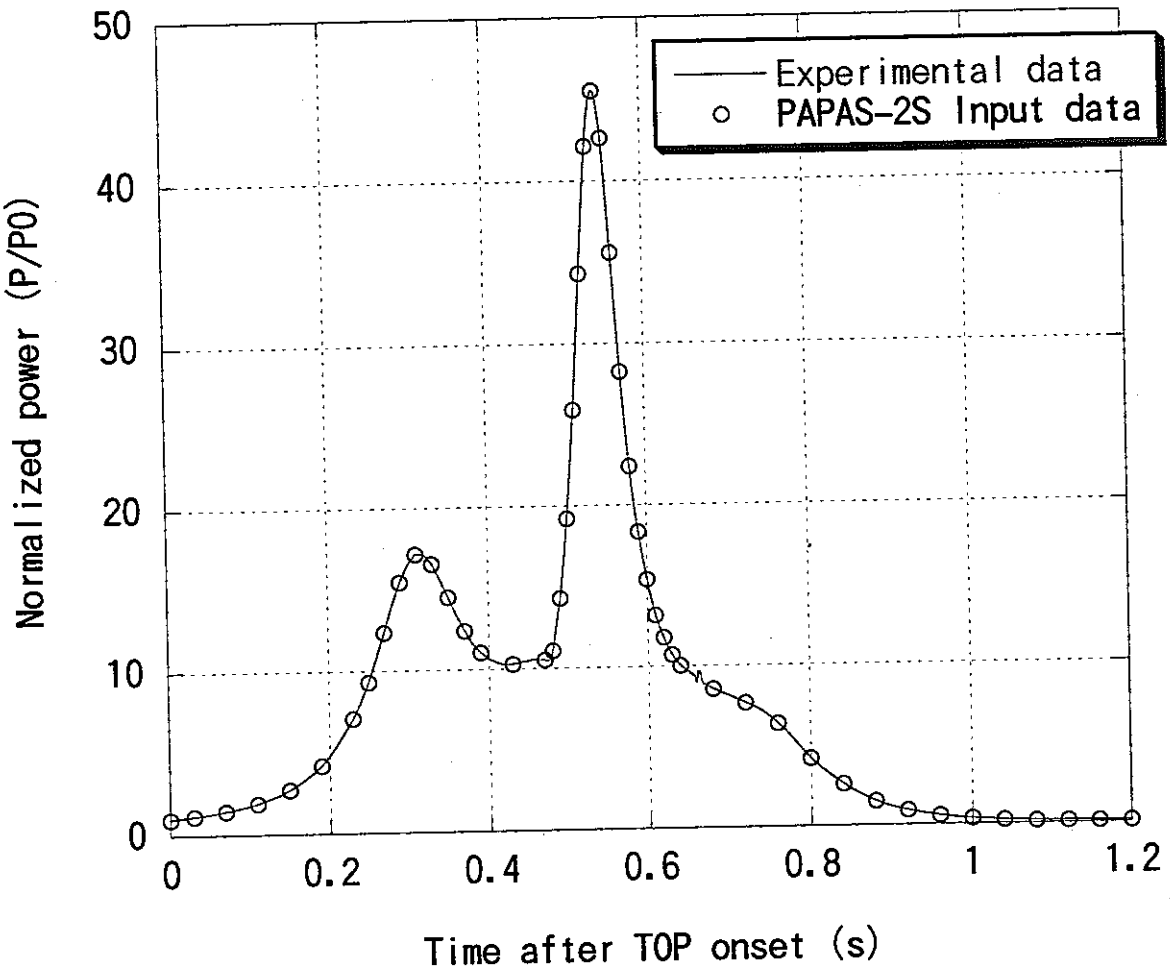

Figure 3 Transient power history used in the PAPAS-2S calculation

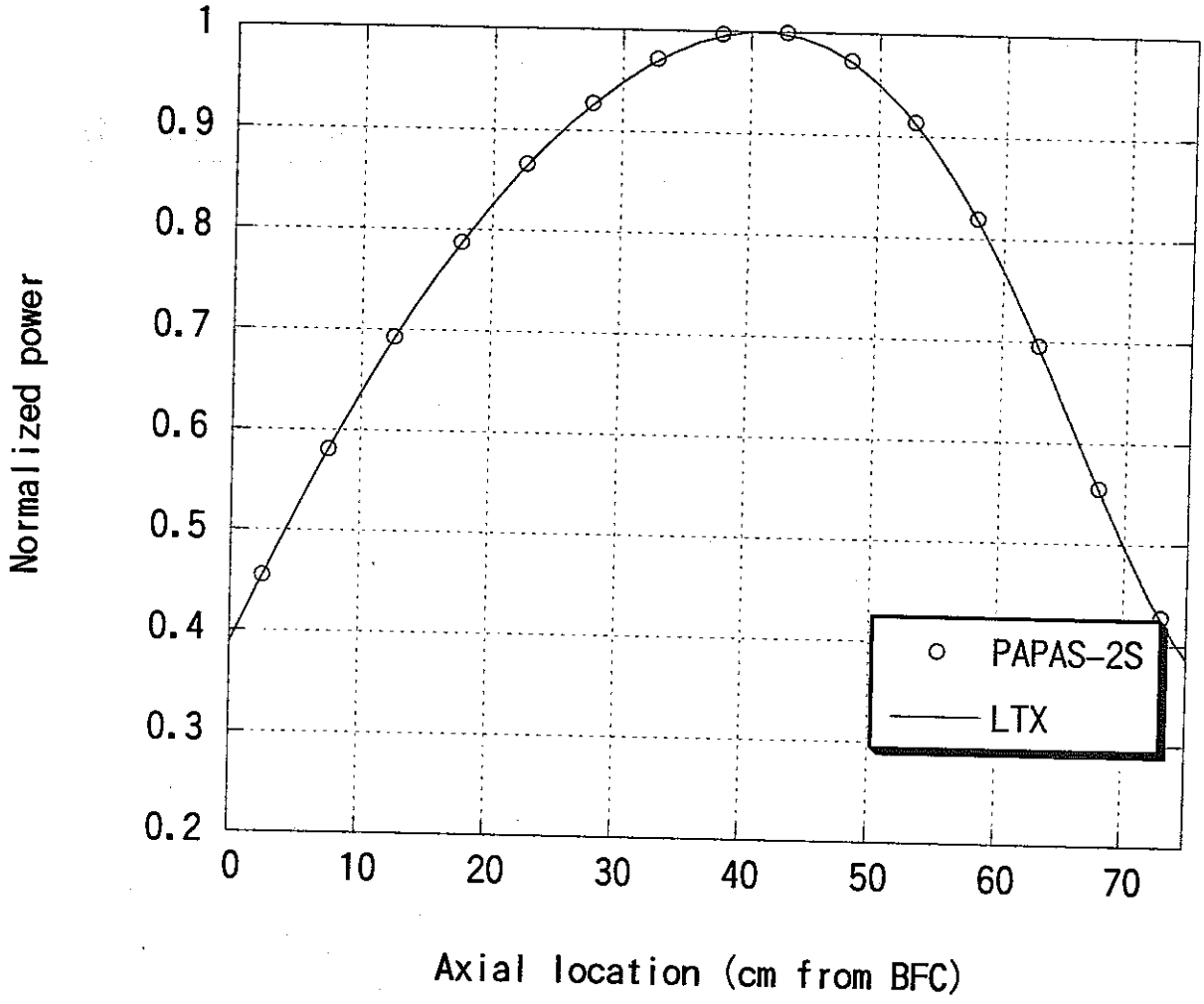

Figure 4 Axial power profile used in the PAPAS-2S code

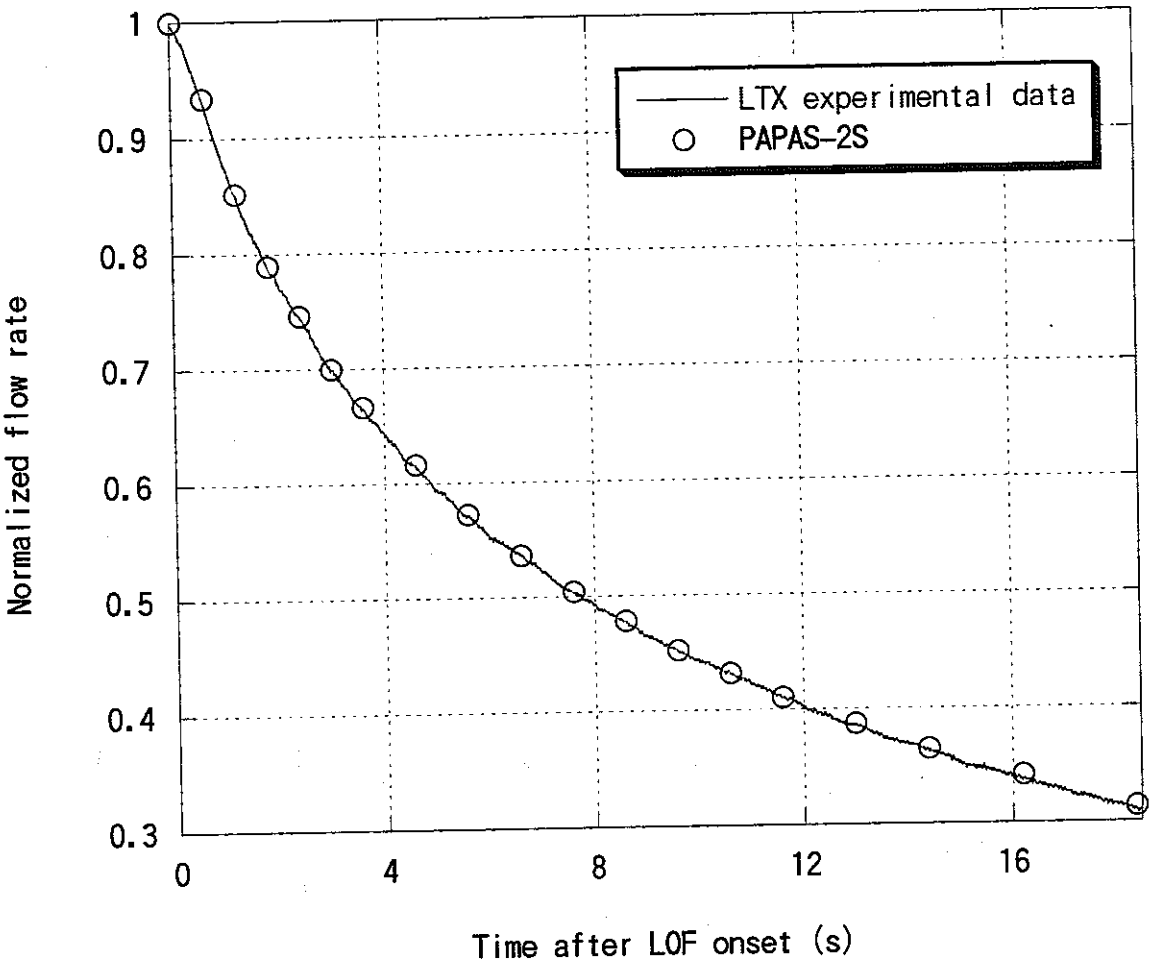

Figure 5 Flow rate history during LOF used in the PAPAS-2S code

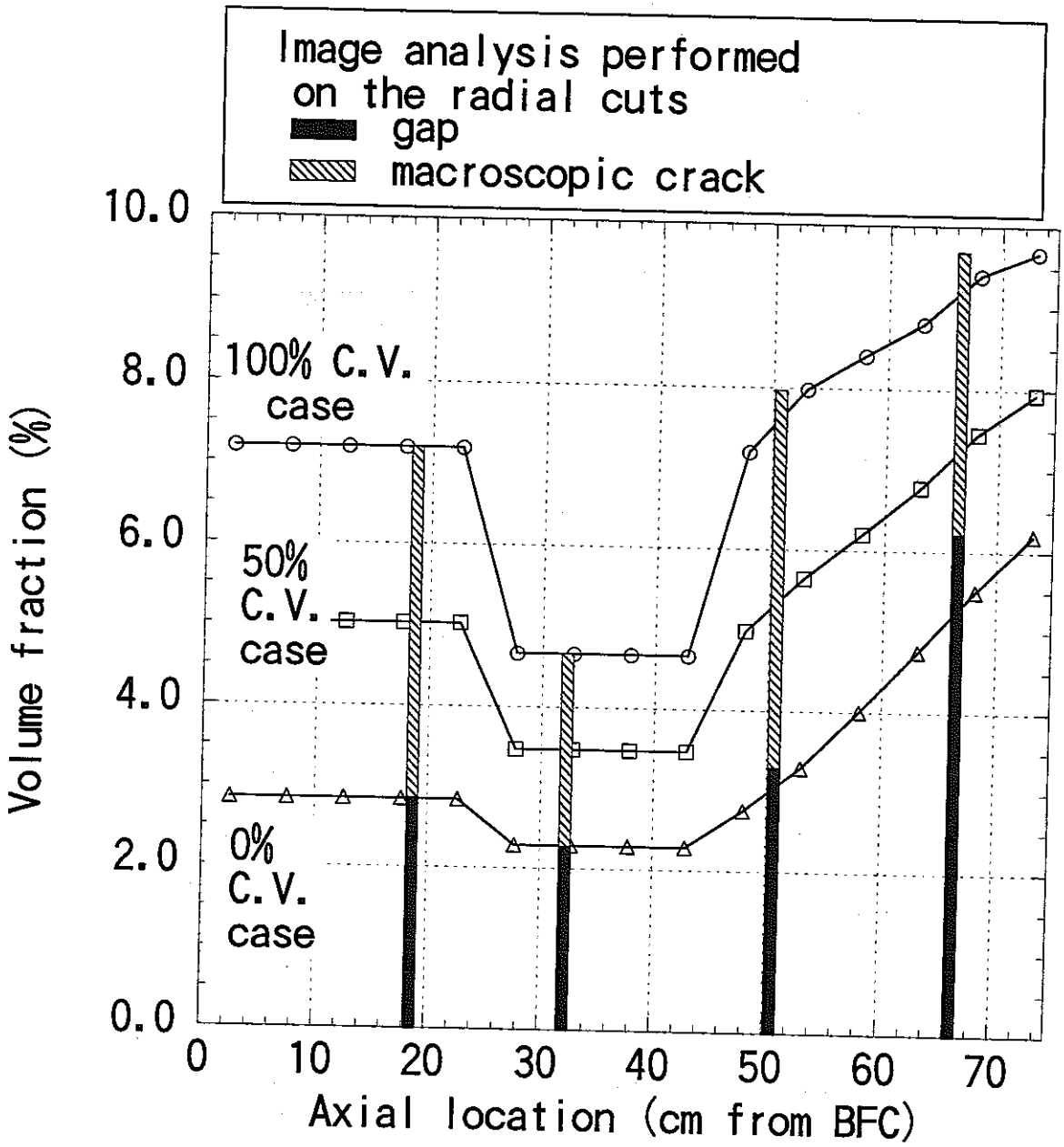

Figure 6 Crack volume availability for PCMI mitigation assumed in PAPAS-2S

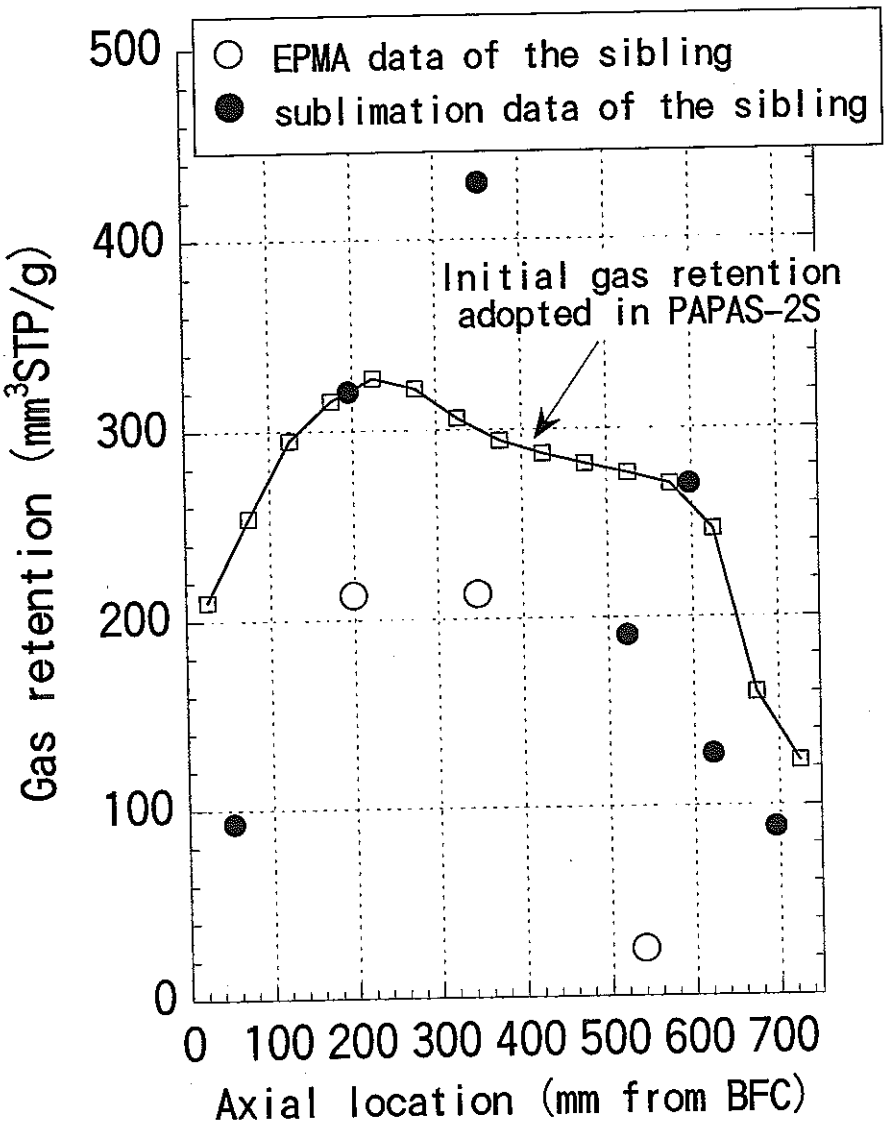

Figure 7 Axial profile of gas retention assumed for the SCARABIX-CABRI type fuel in PAPAS-2S

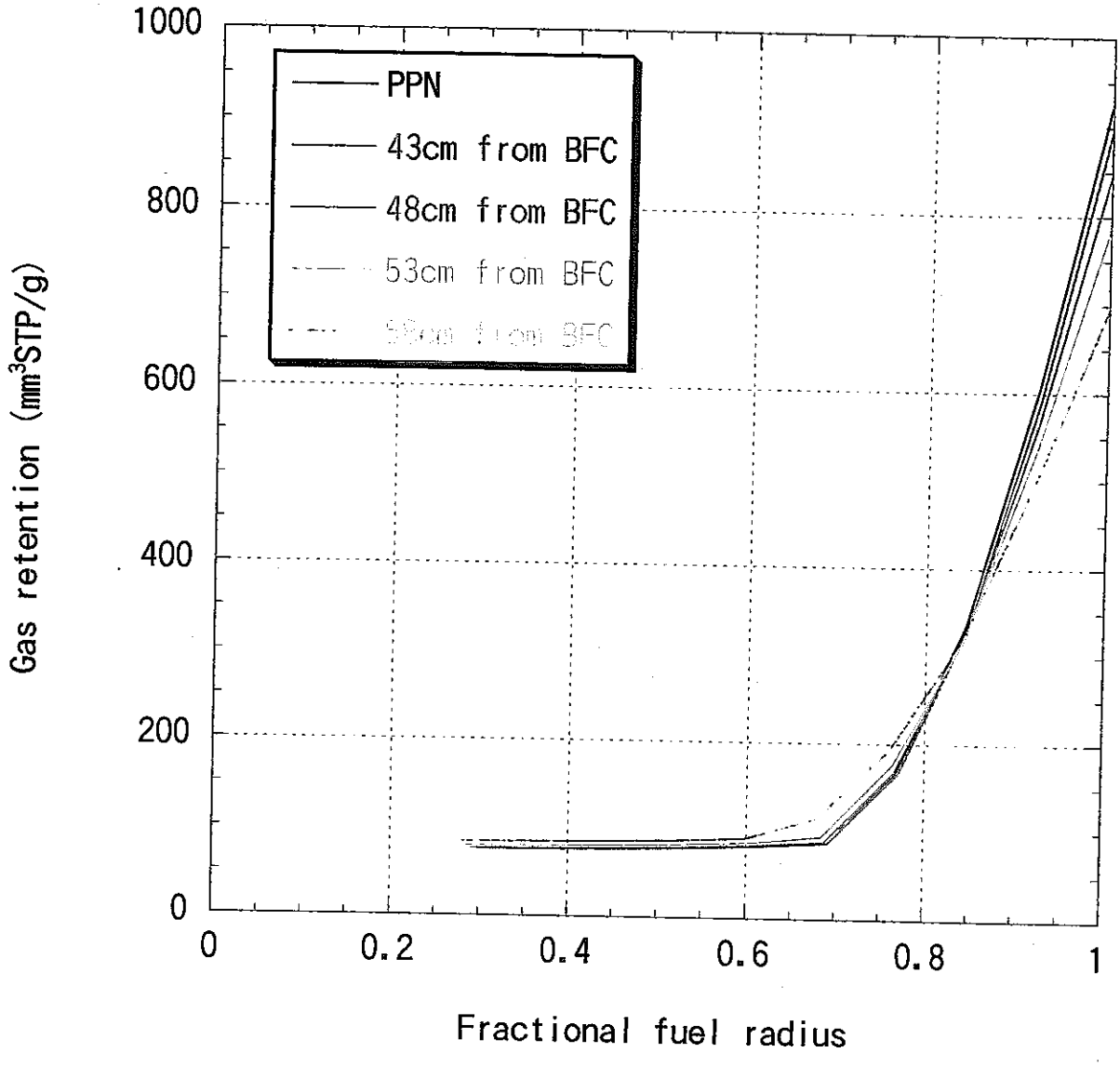

Figure 8 Radial profile of gas retention assumed for the SCARABIX-CABRI type fuel in PAPAS-2S

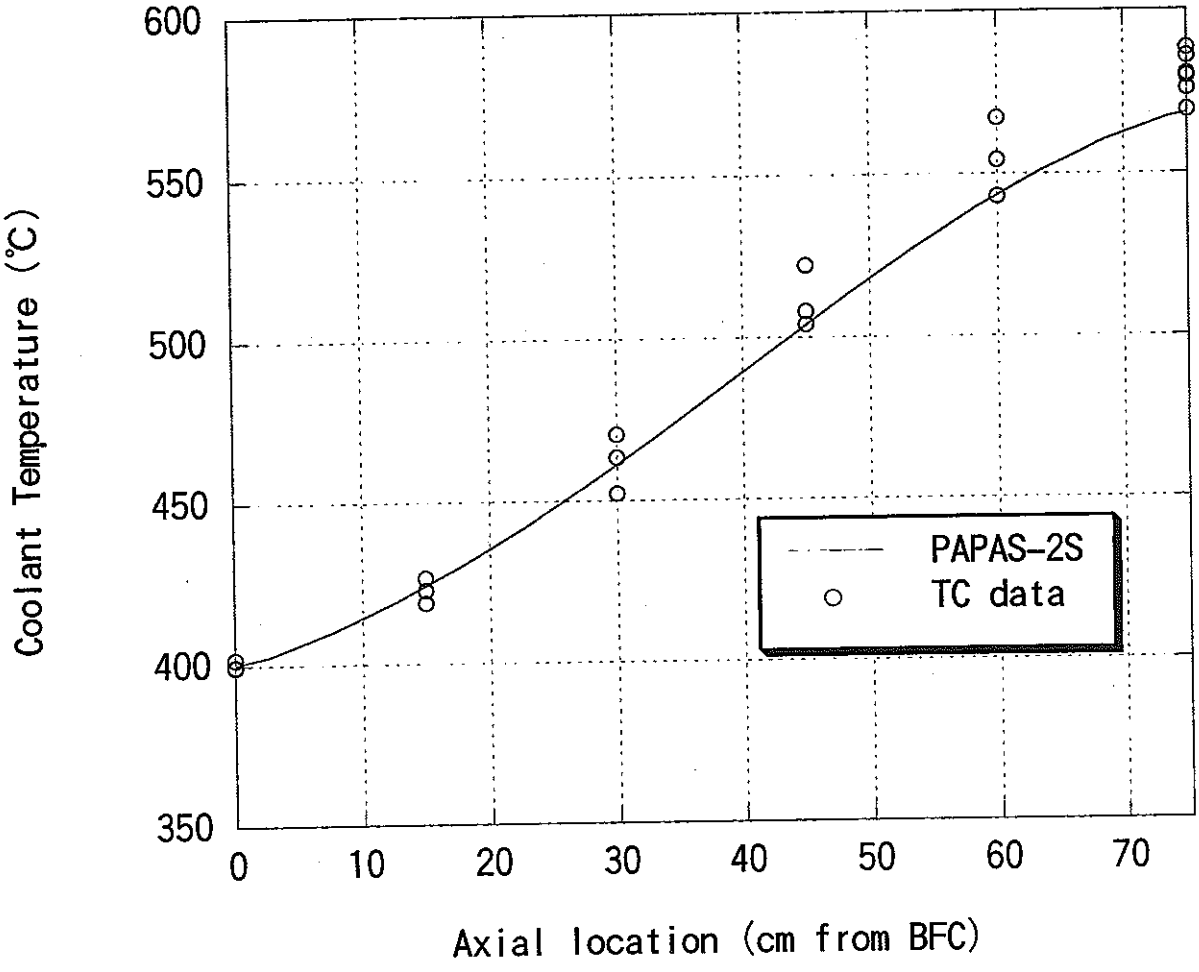

Figure 9 Coolant temperature profile at steady state calculated in the PAPAS-2S code

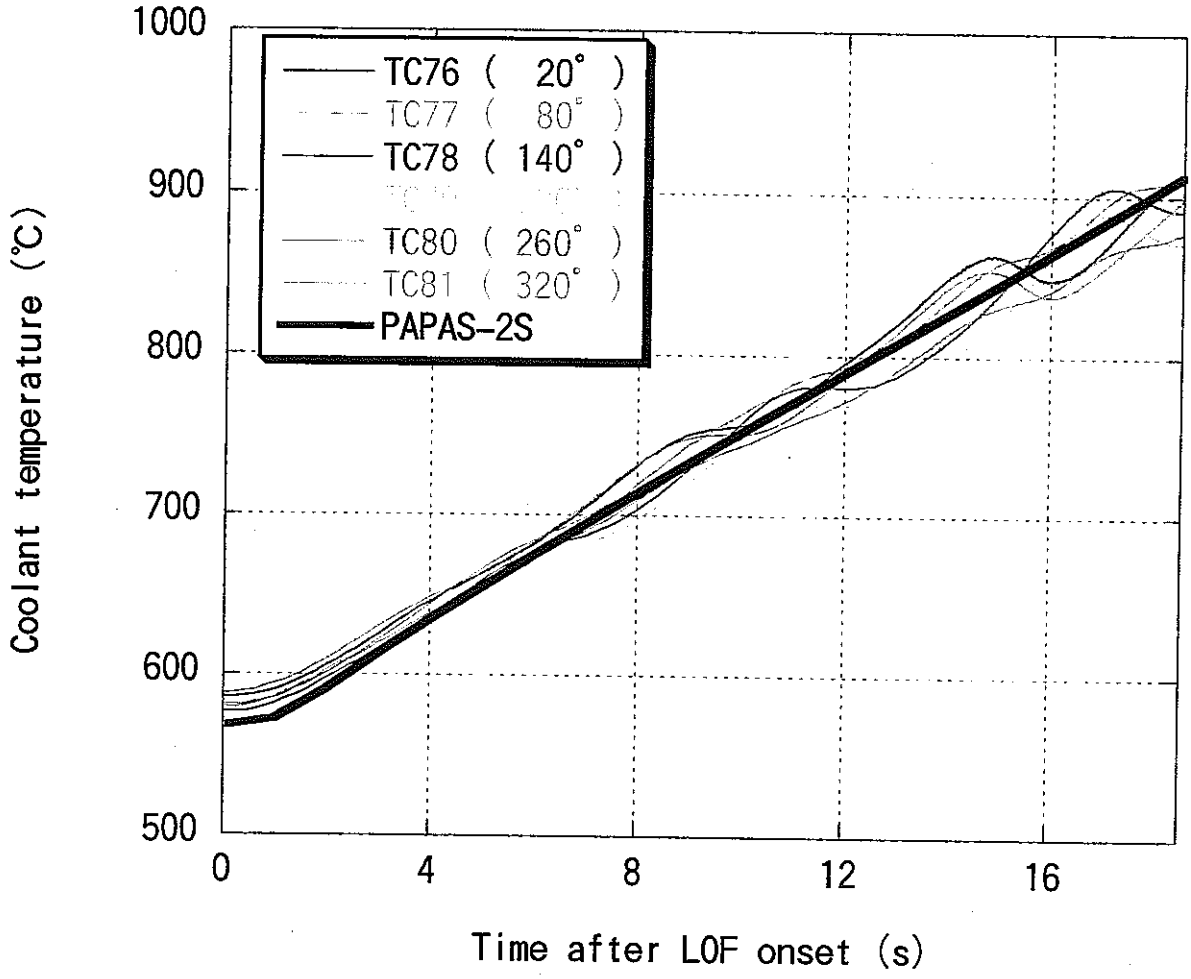

Figure 10 Calculated coolant temperature history at TFC during LOF

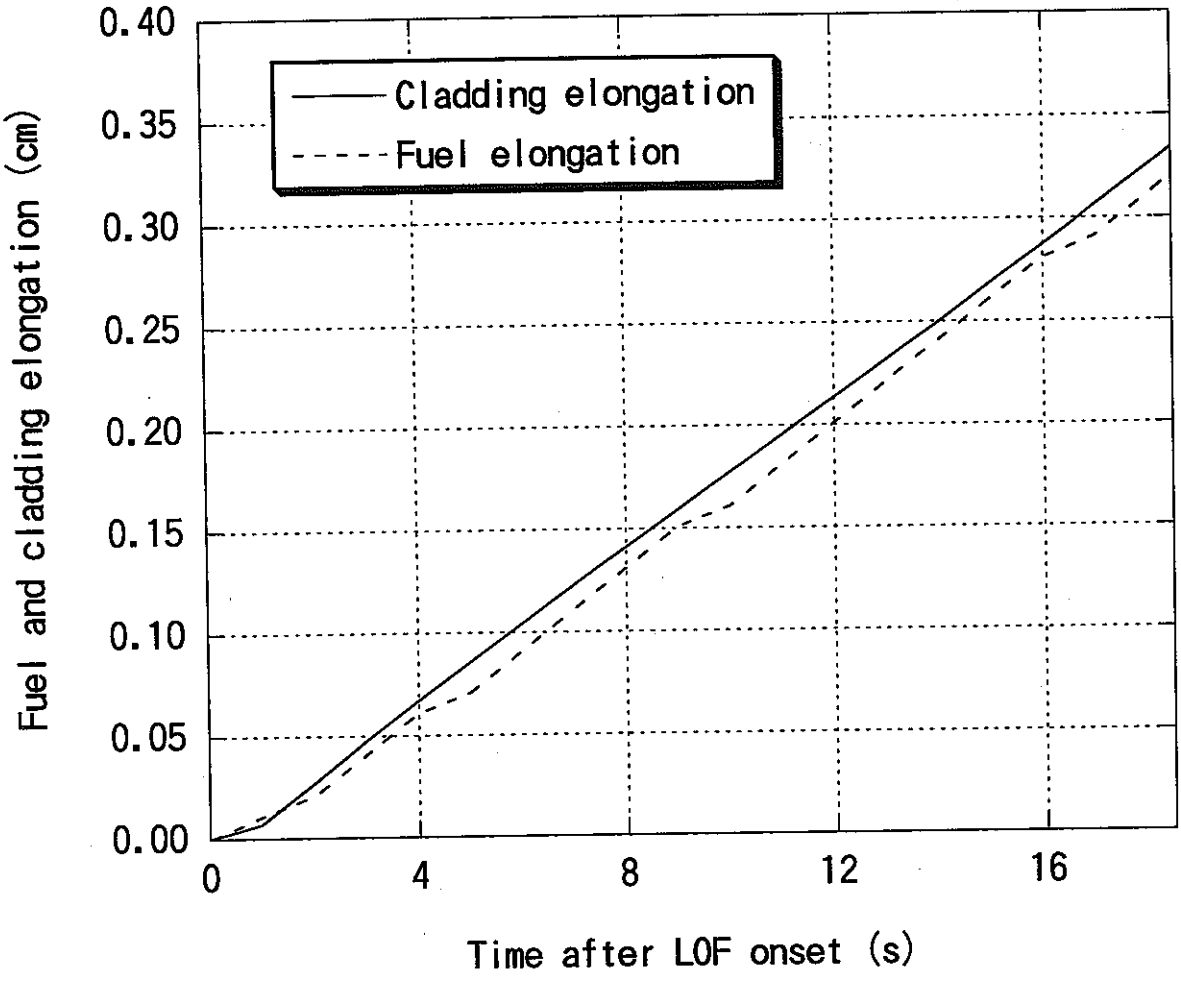

Figure 11 Fuel and cladding elongation during LOF up to TOP onset calculated by PAPAS-2S

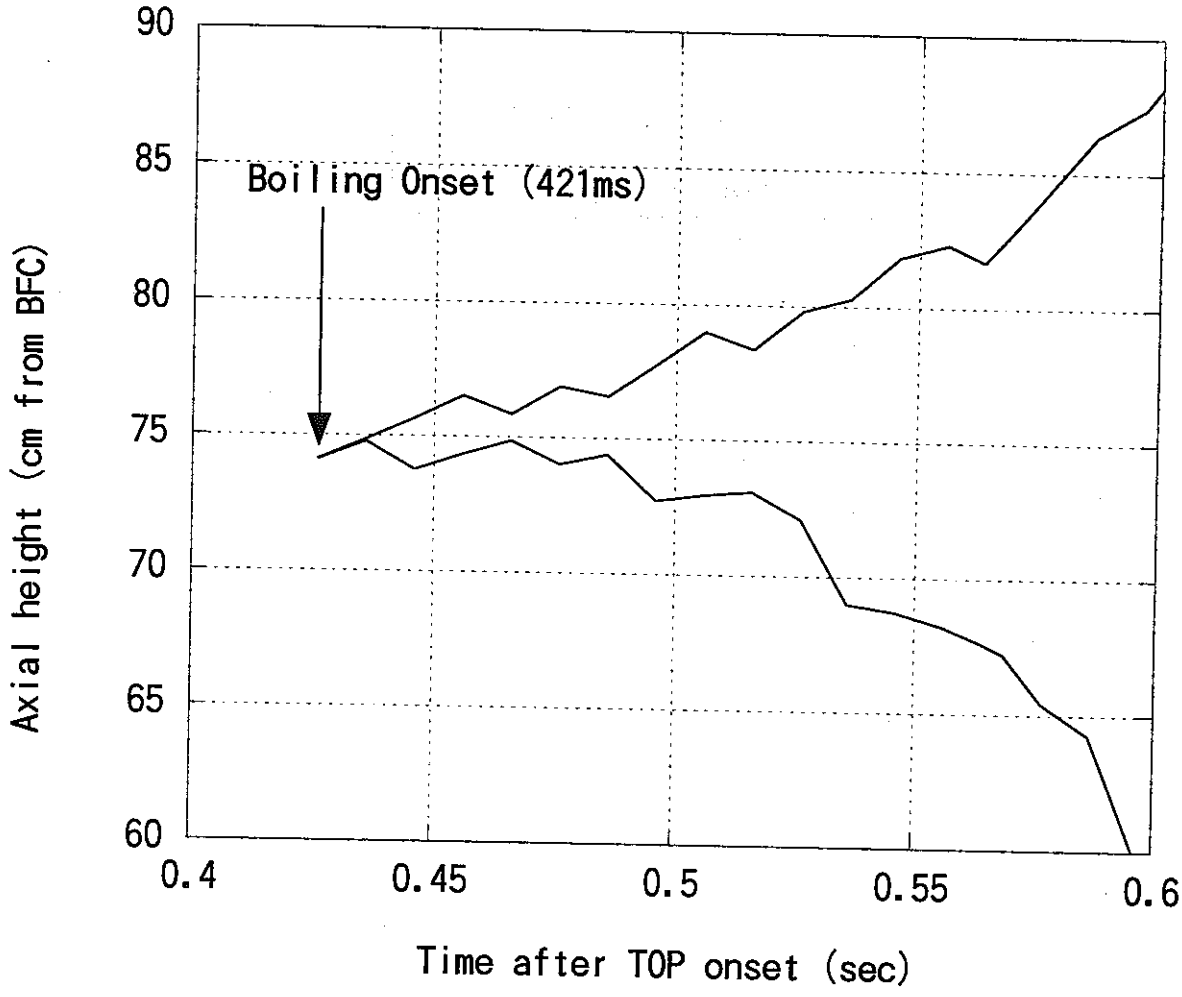

Figure 12 Coolant boiling initiation and voiding zone extension calculated in PAPAS-2S

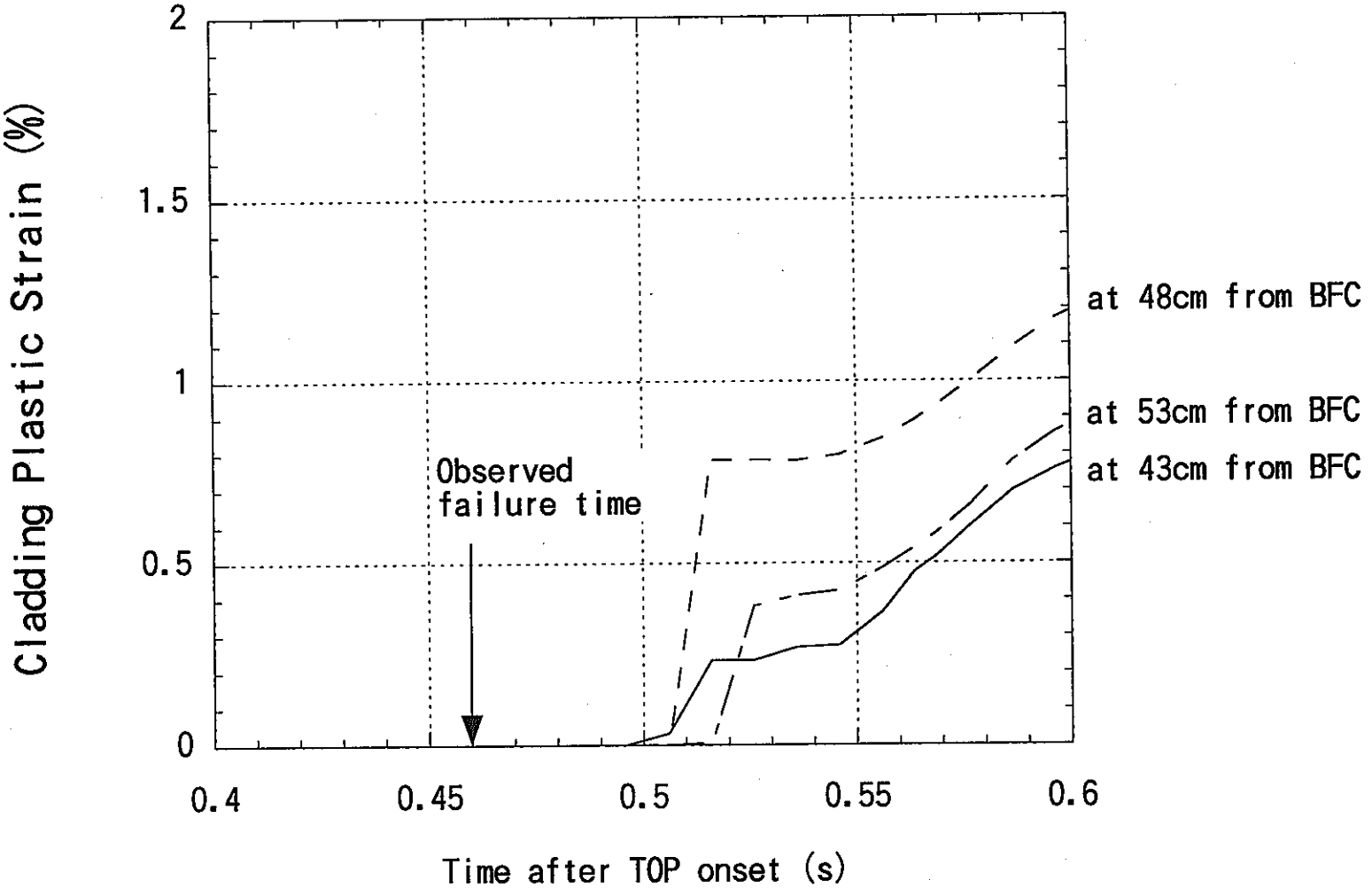

Figure 13 Cladding plastic strain calculated in the "100% gap and 100% crack volume availability" case

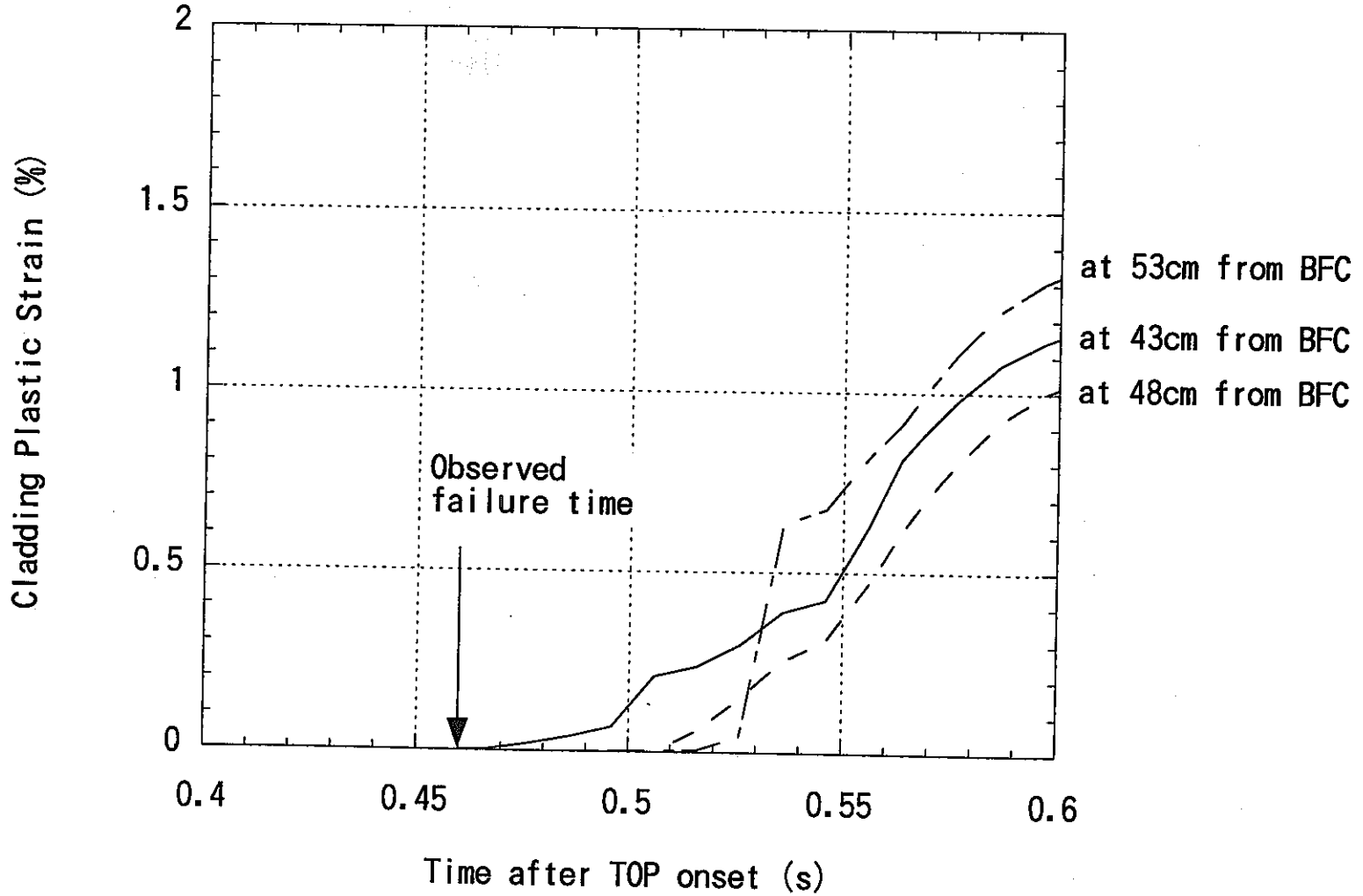

Figure 14 Cladding plastic strain calculated in the "100% gap and 50% crack volume availability" case

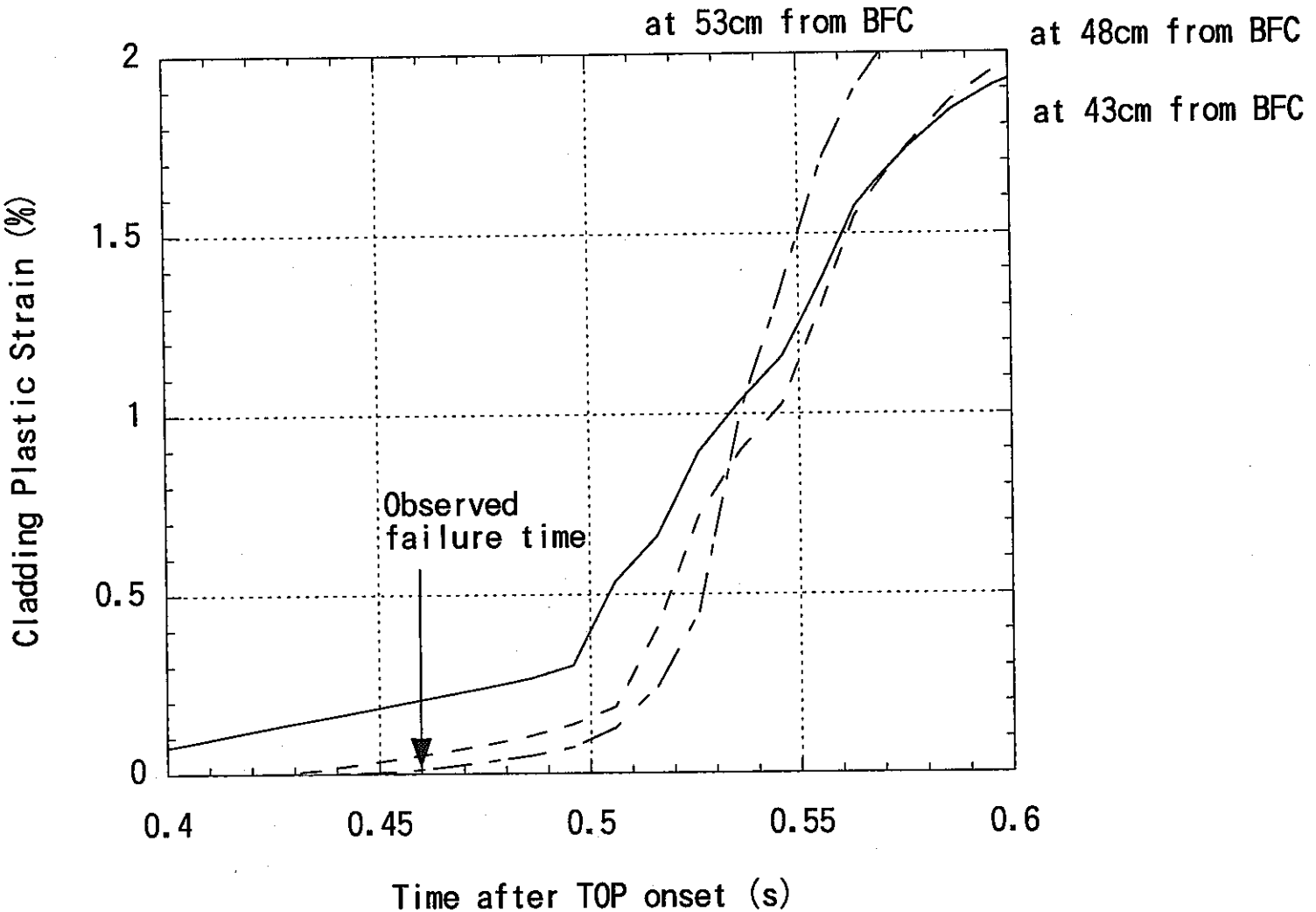

Figure 15 Cladding plastic strain calculated in the "100% gap and 0% crack volume availability" case

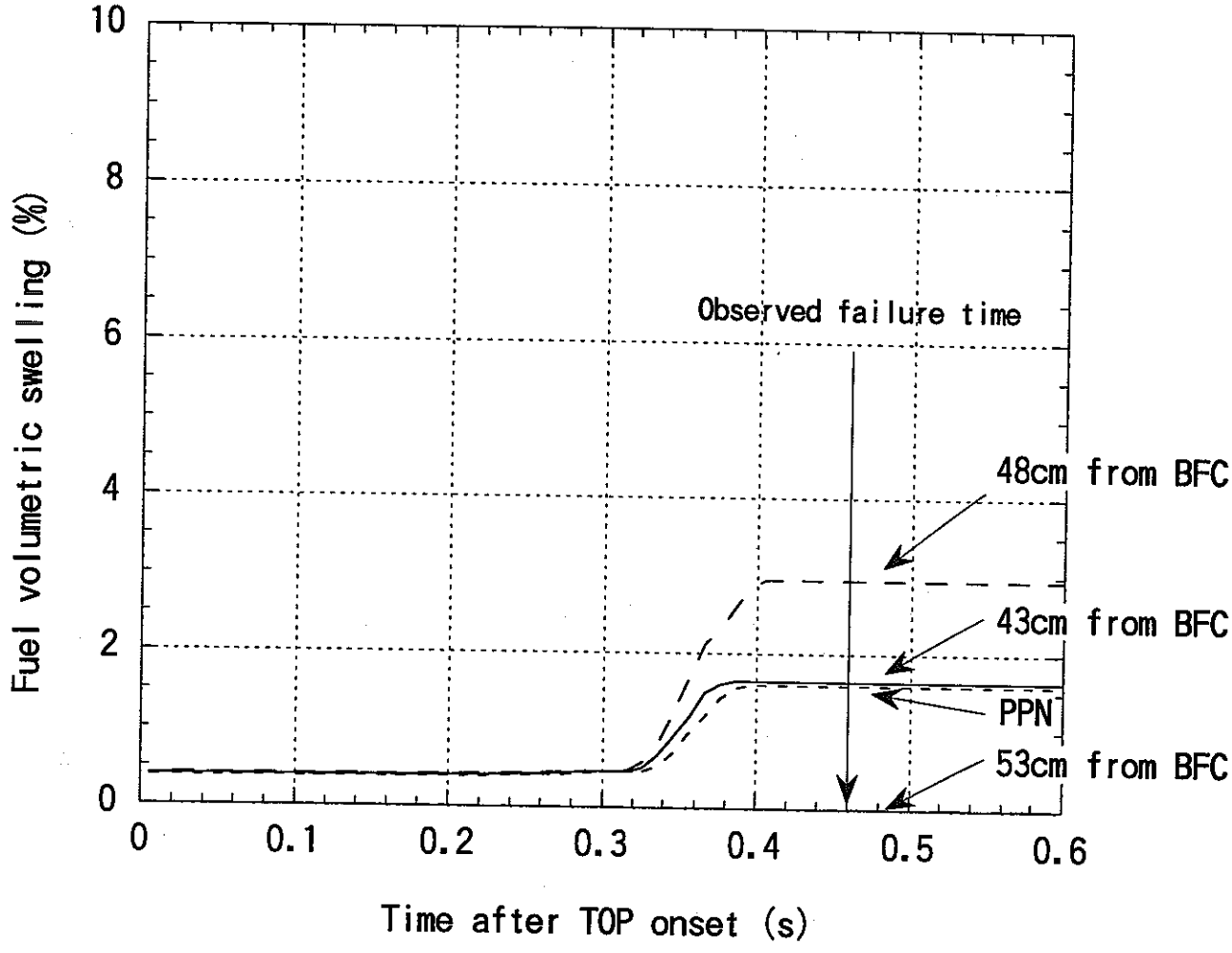

Figure 16 Fuel volumetric swelling calculated by PAPAS-2S around the fractional fuel radius of 0.7 during TOP

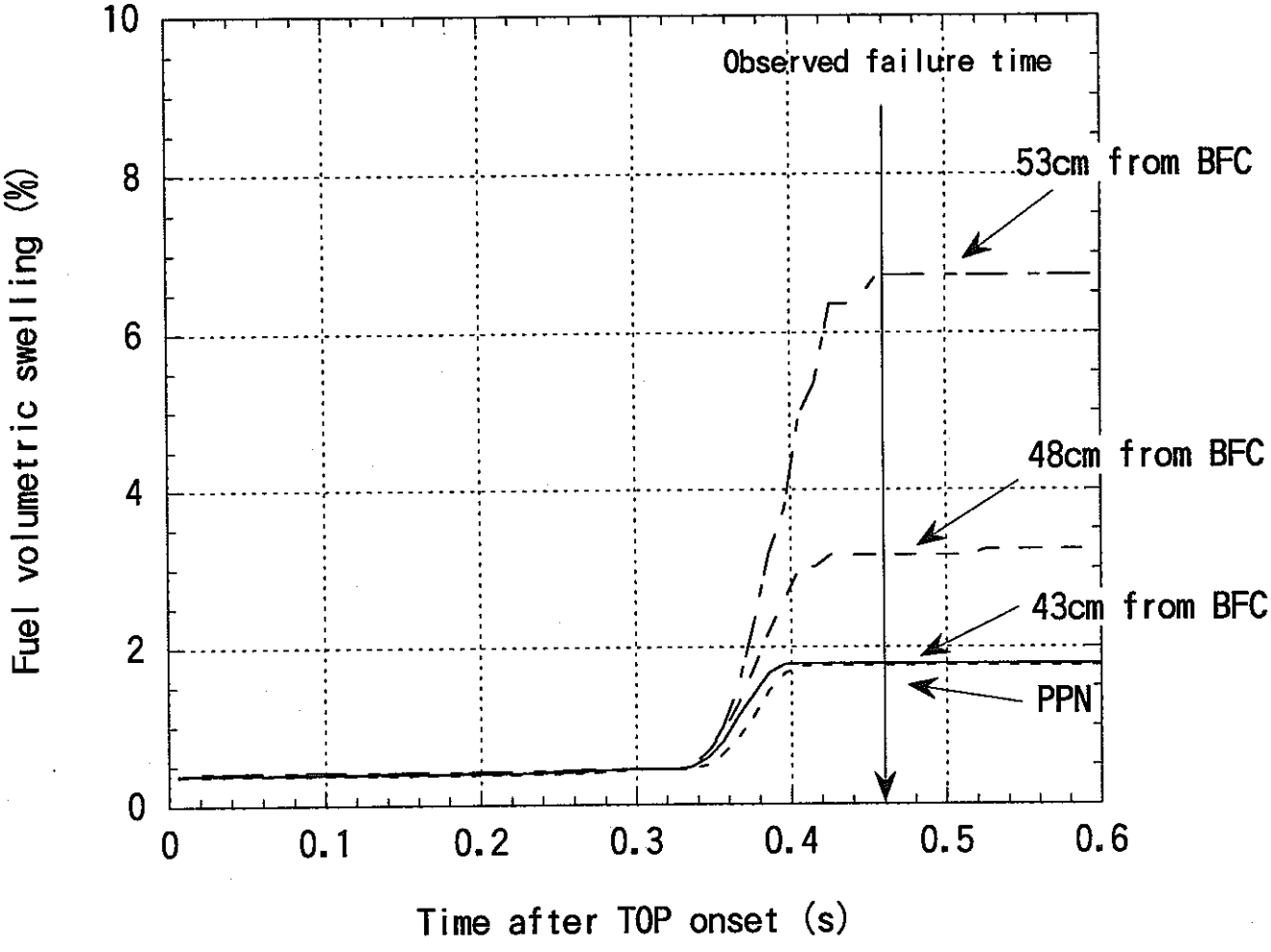

Figure 17 Fuel volumetric swelling calculated by PAPAS-2S around the fractional fuel radius of 0.8 during TOP

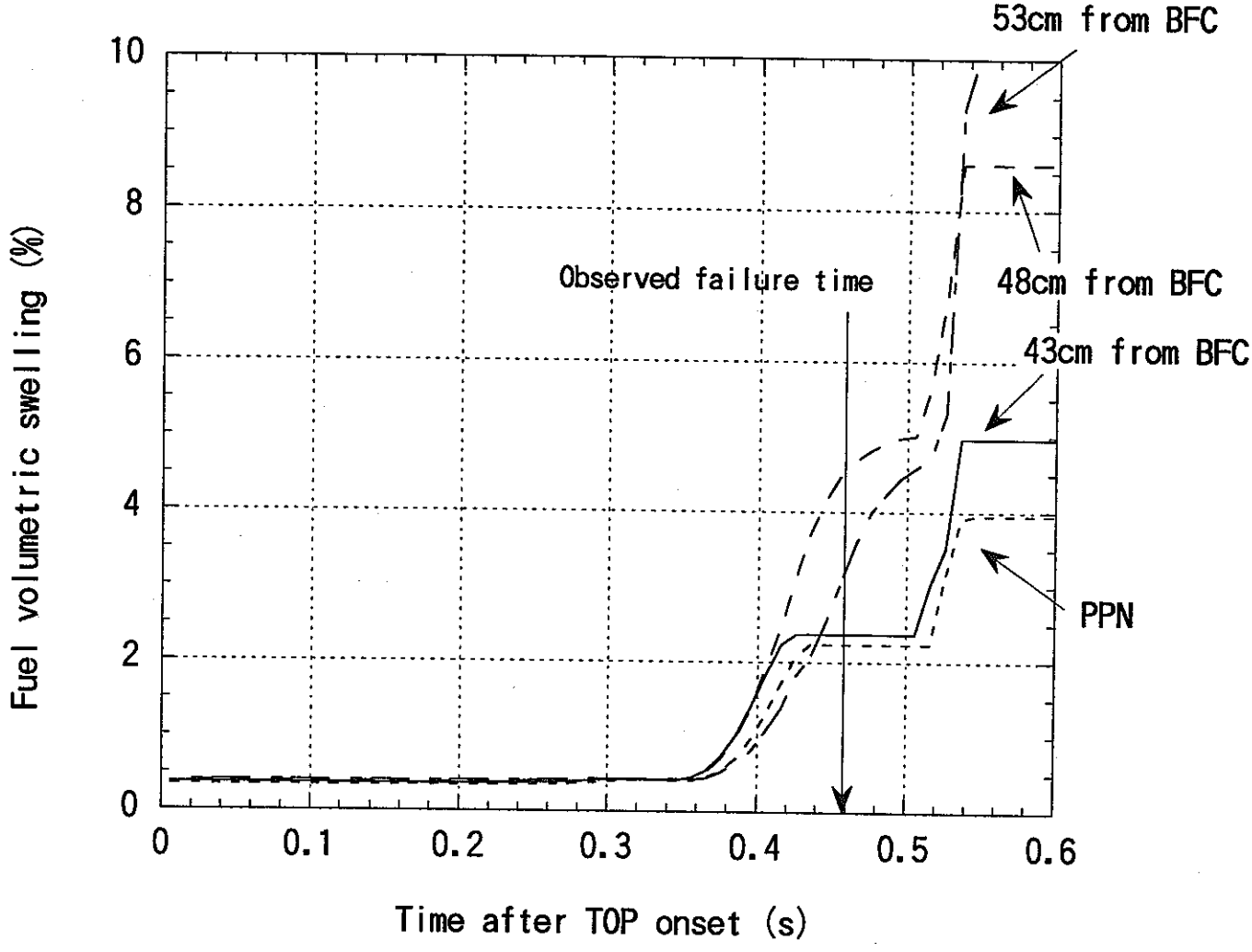

Figure 18 Fuel volumetric swelling calculated by PAPAS-2S around the fractional fuel radius of 0.9 during TOP

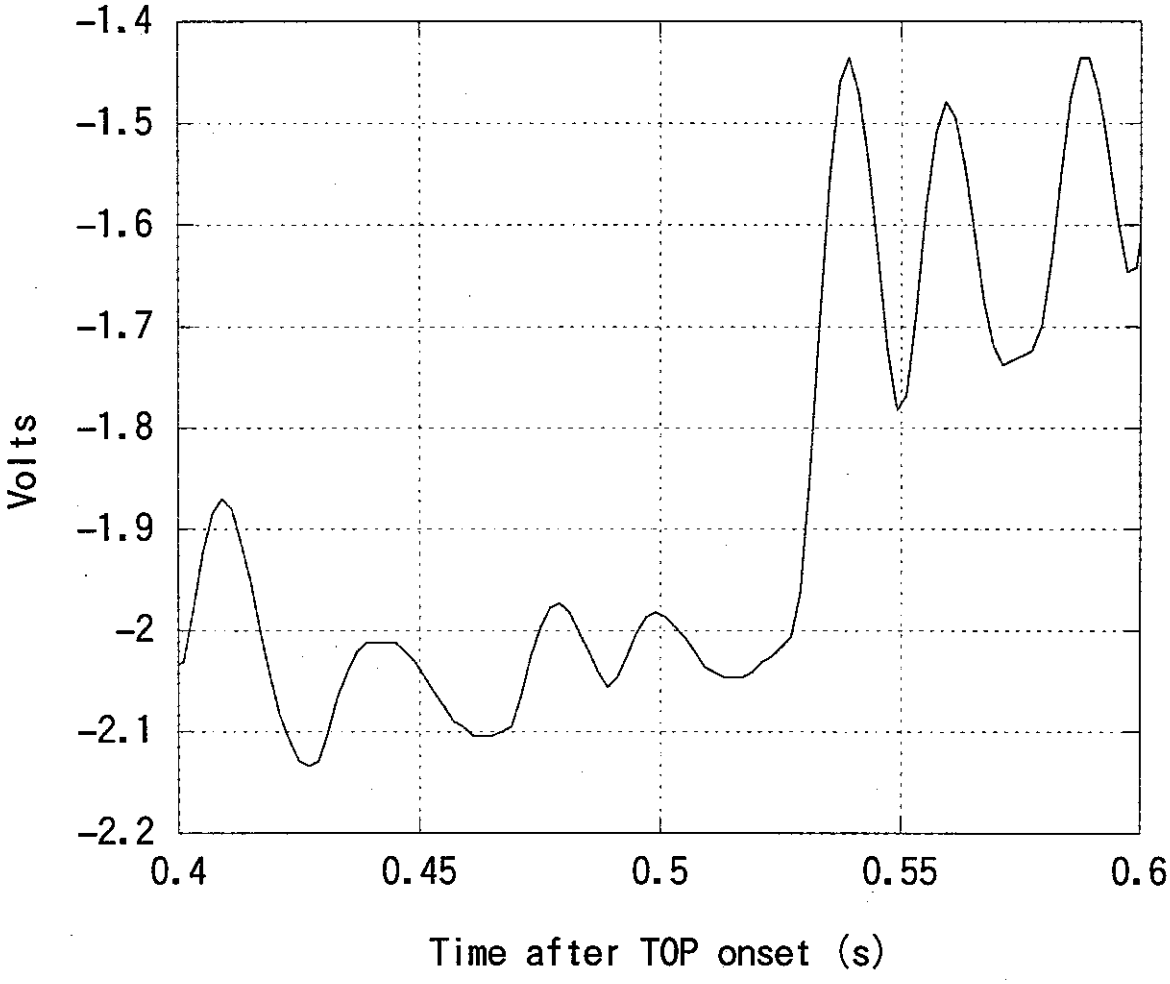

Figure19 DT signal history during TOP in the LTX test

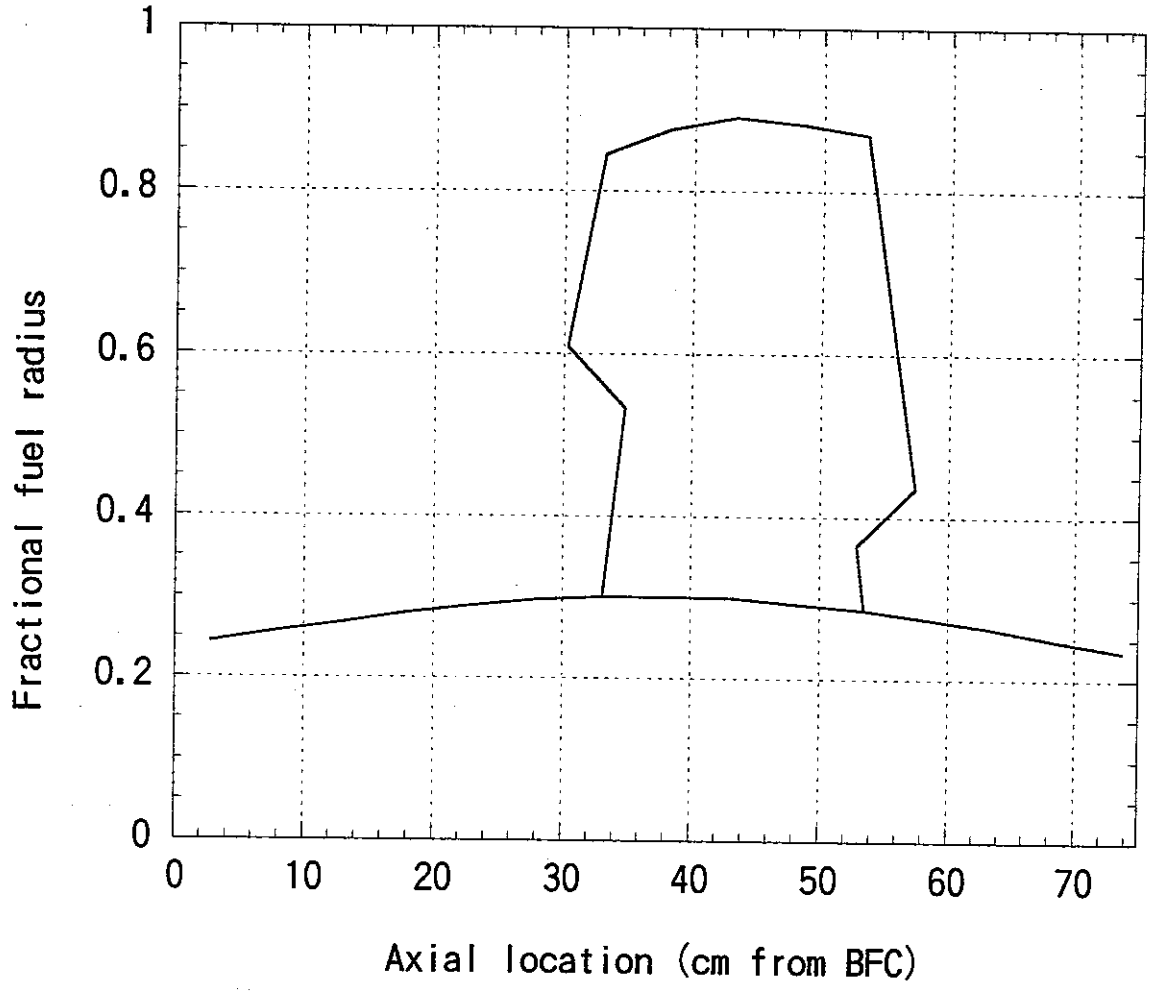

Figure 20 Fuel melting boundary at the sudden pin top displacement observed by the special DT (at 526ms after TOP onset)

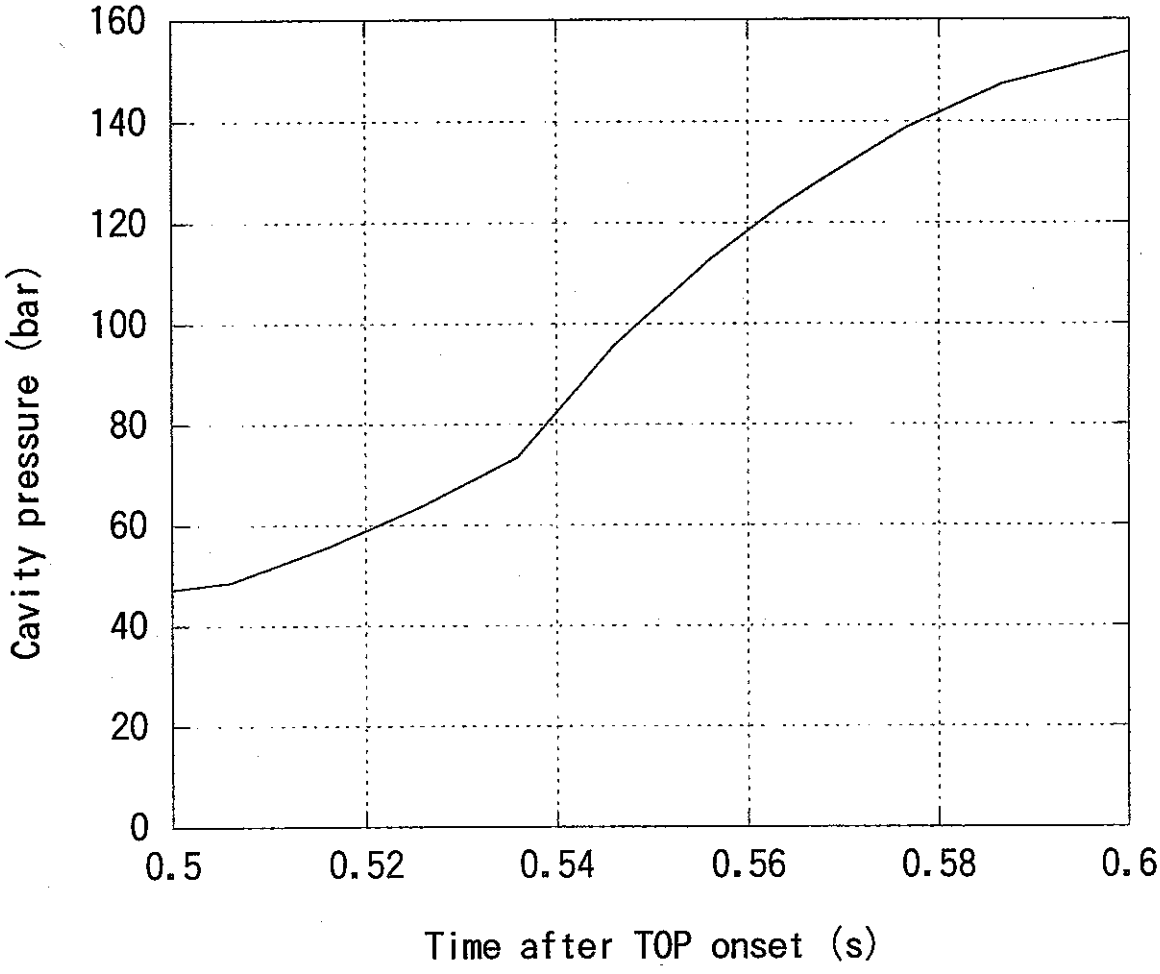

Figure21 Molten cavity pressure history during TOP calculated by PAPAS-2S

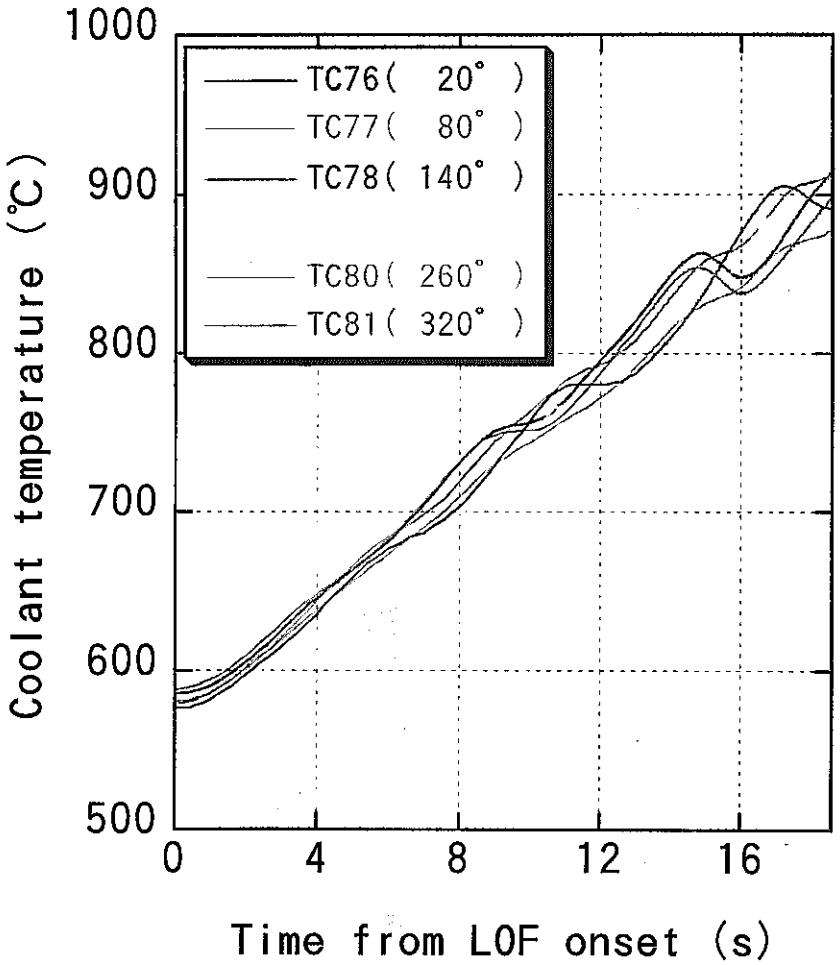

LTX test

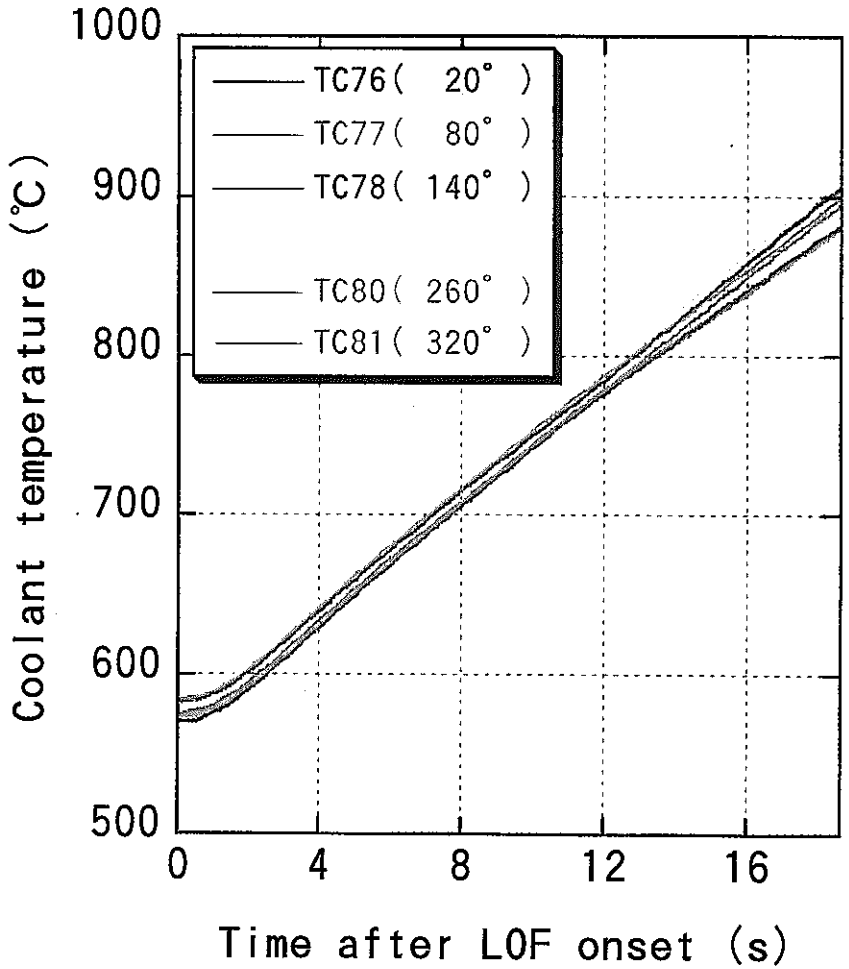

LT4 test

Figure 22 Comparison of coolant temperature at TFC during LOF between the LTX and LT4 tests

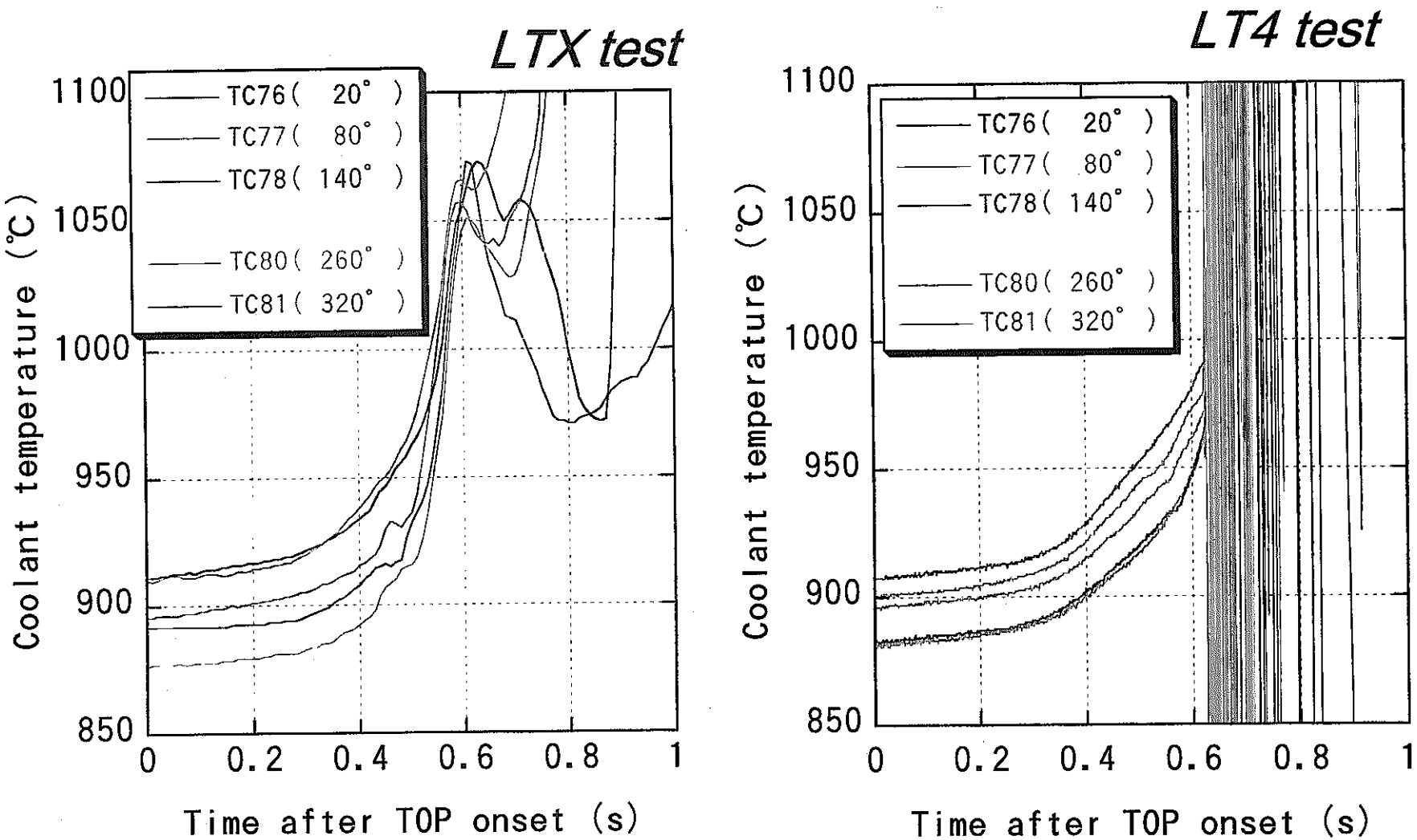

Figure 23 Comparison of coolant temperature at TFC during TOP between the LTX and LT4 tests

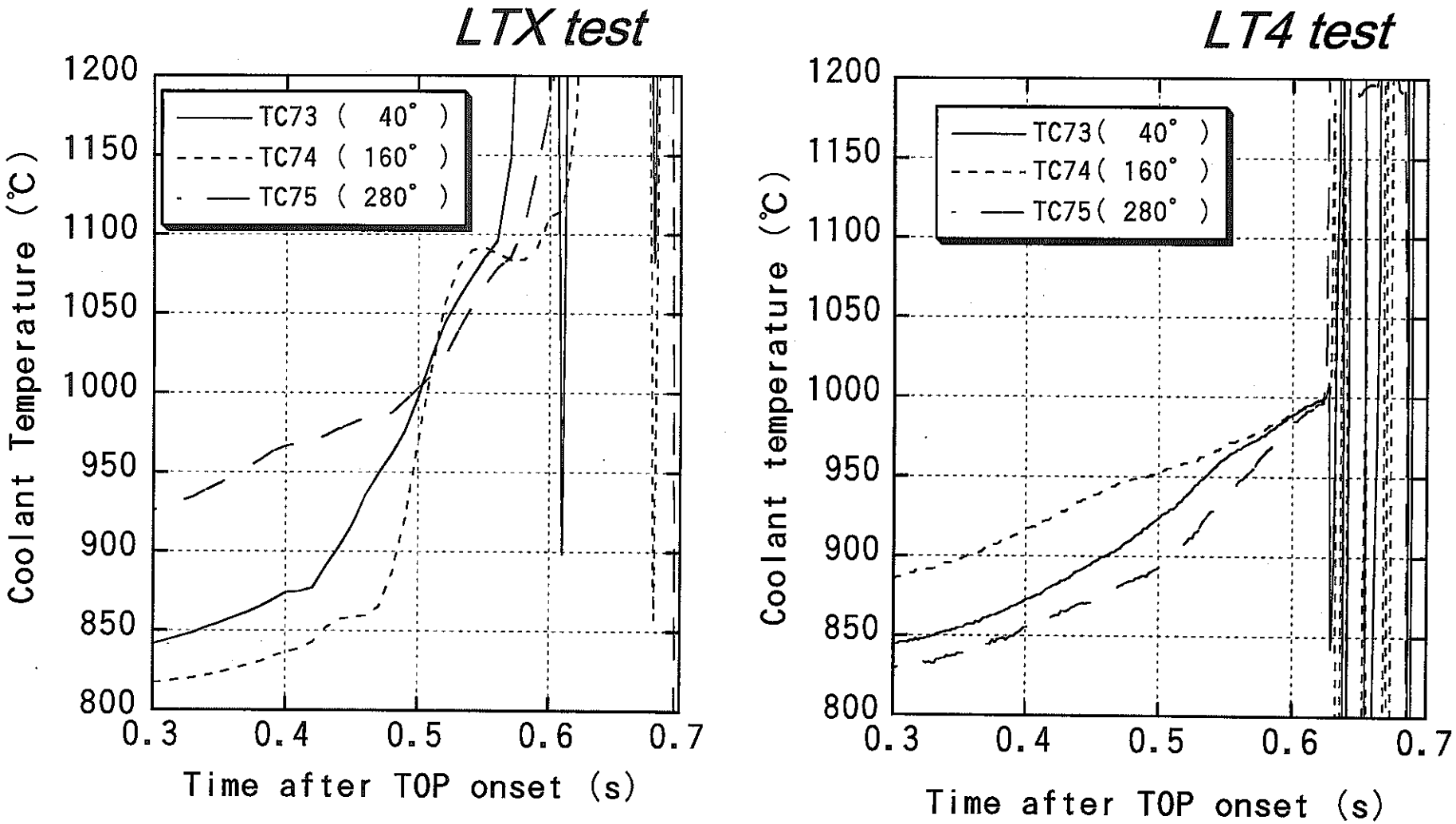

Figure 24 Comparison of coolant temperature at 60 cm/BFC during TOP between the LTX and LT4 tests

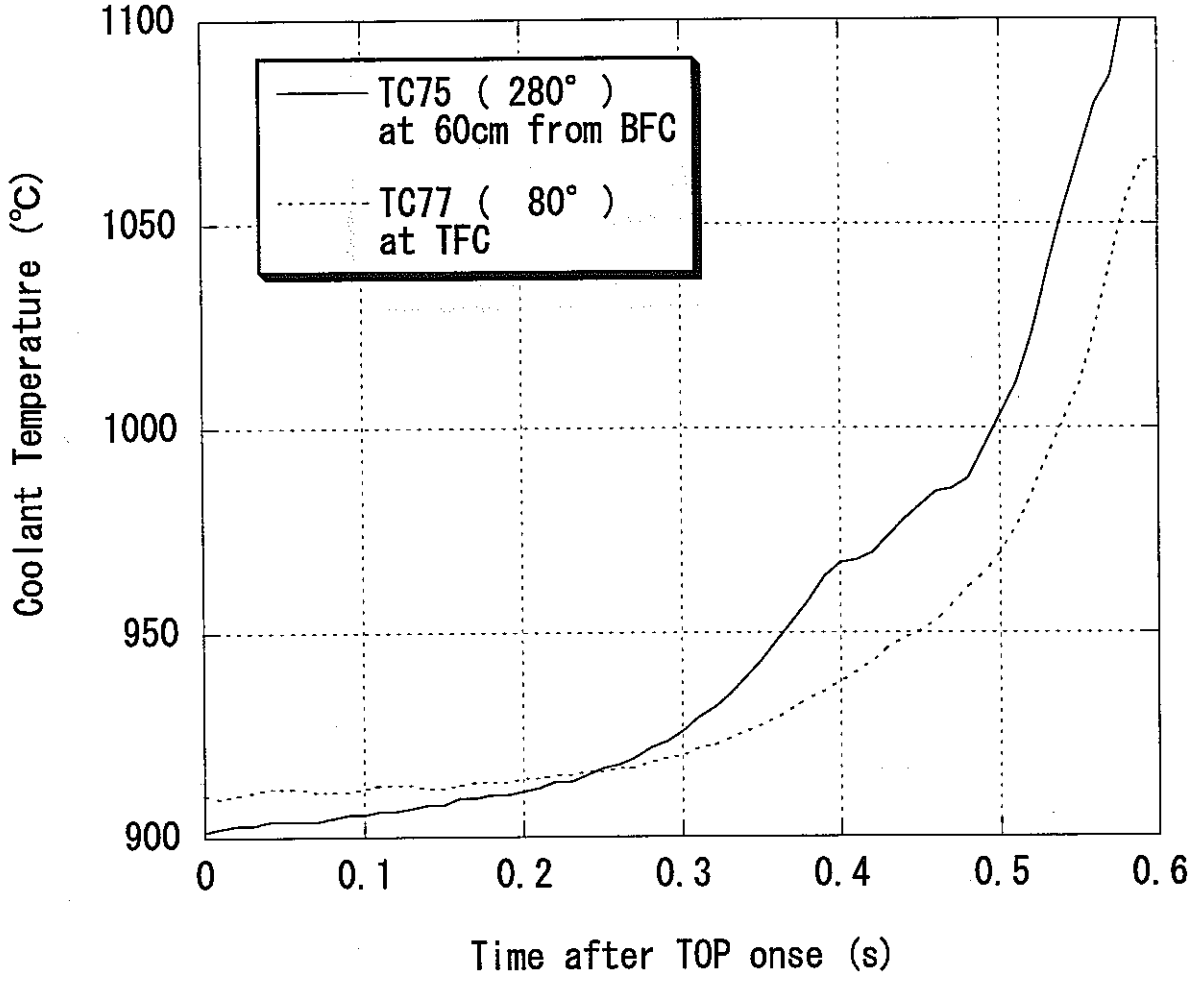

Figure 25 Comparison of coolant temperature history of the hottest azimuth at TFC and 60cm/BFC

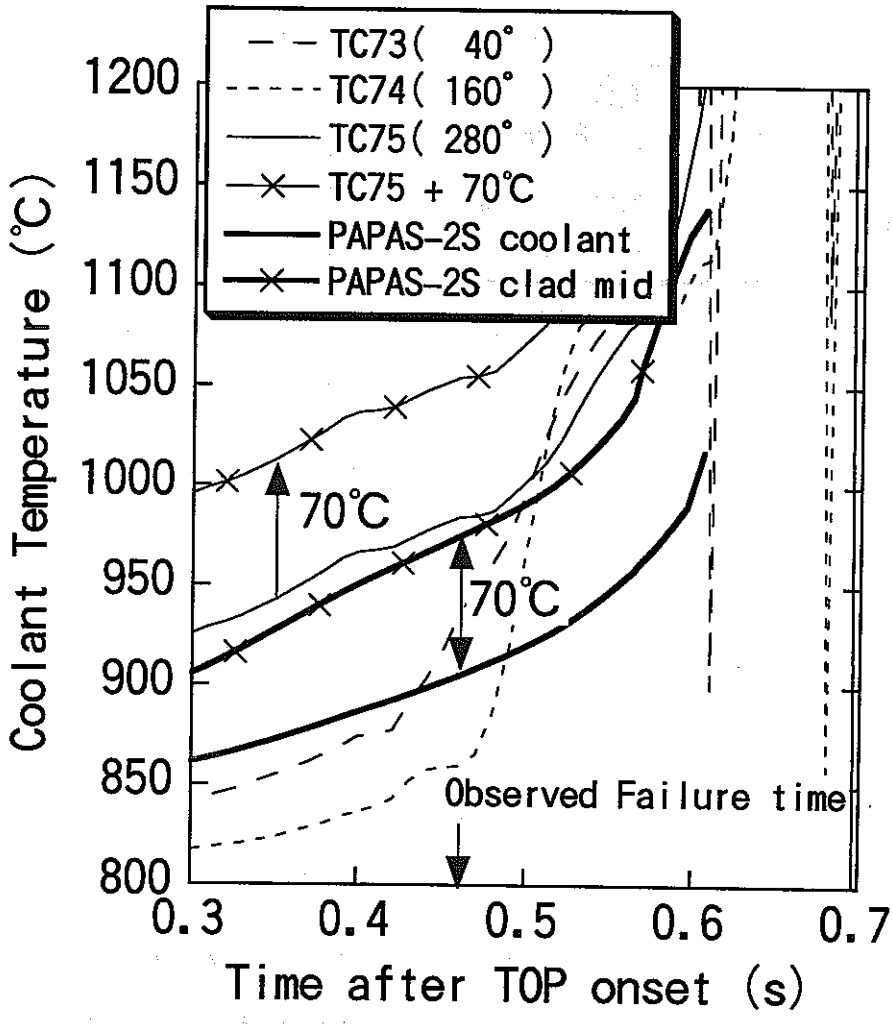

Figure 26 Cladding temperature at the hottest azimuth

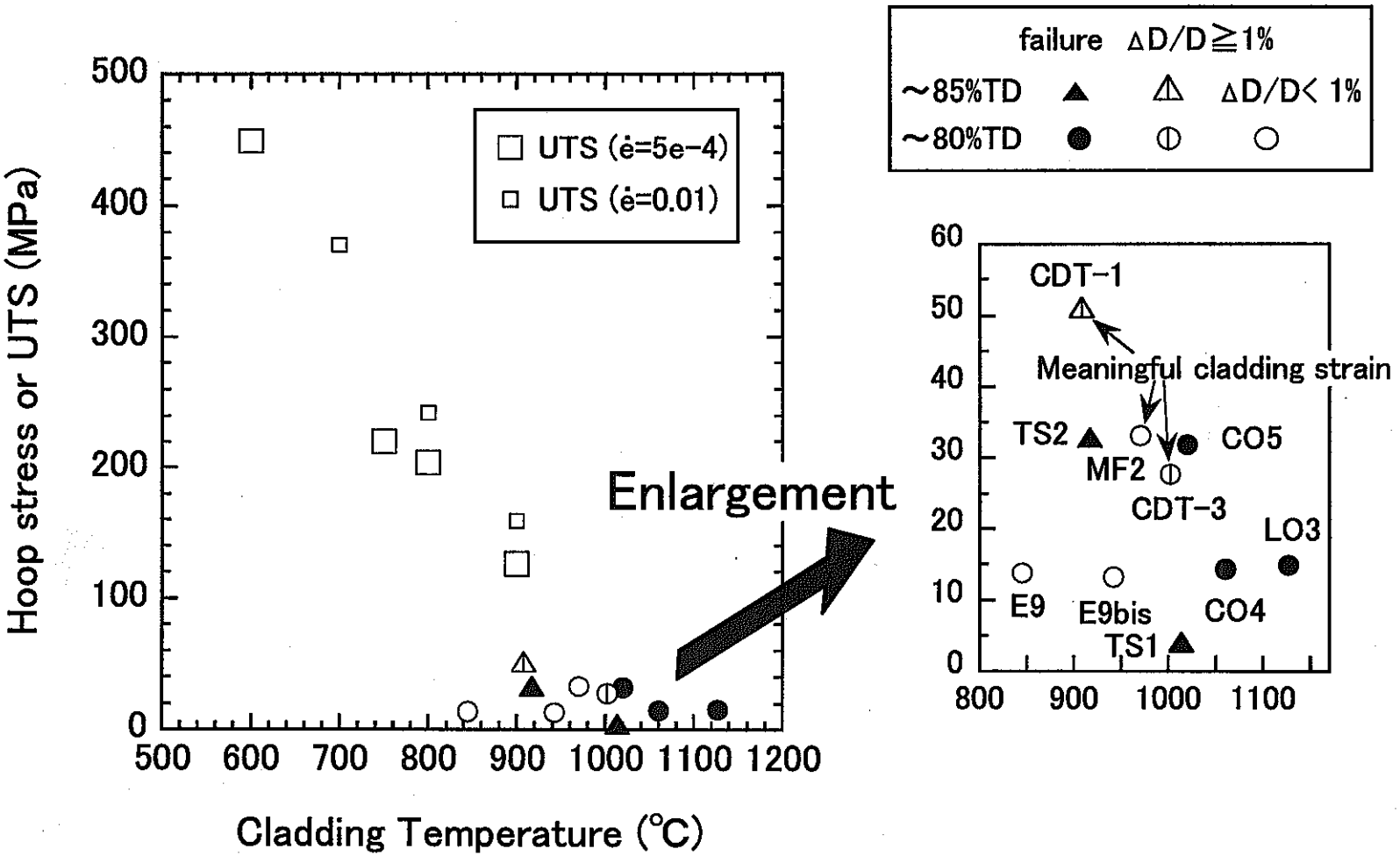

Figure 27 Failure condition of slow-TOP tests with low smear density fuels

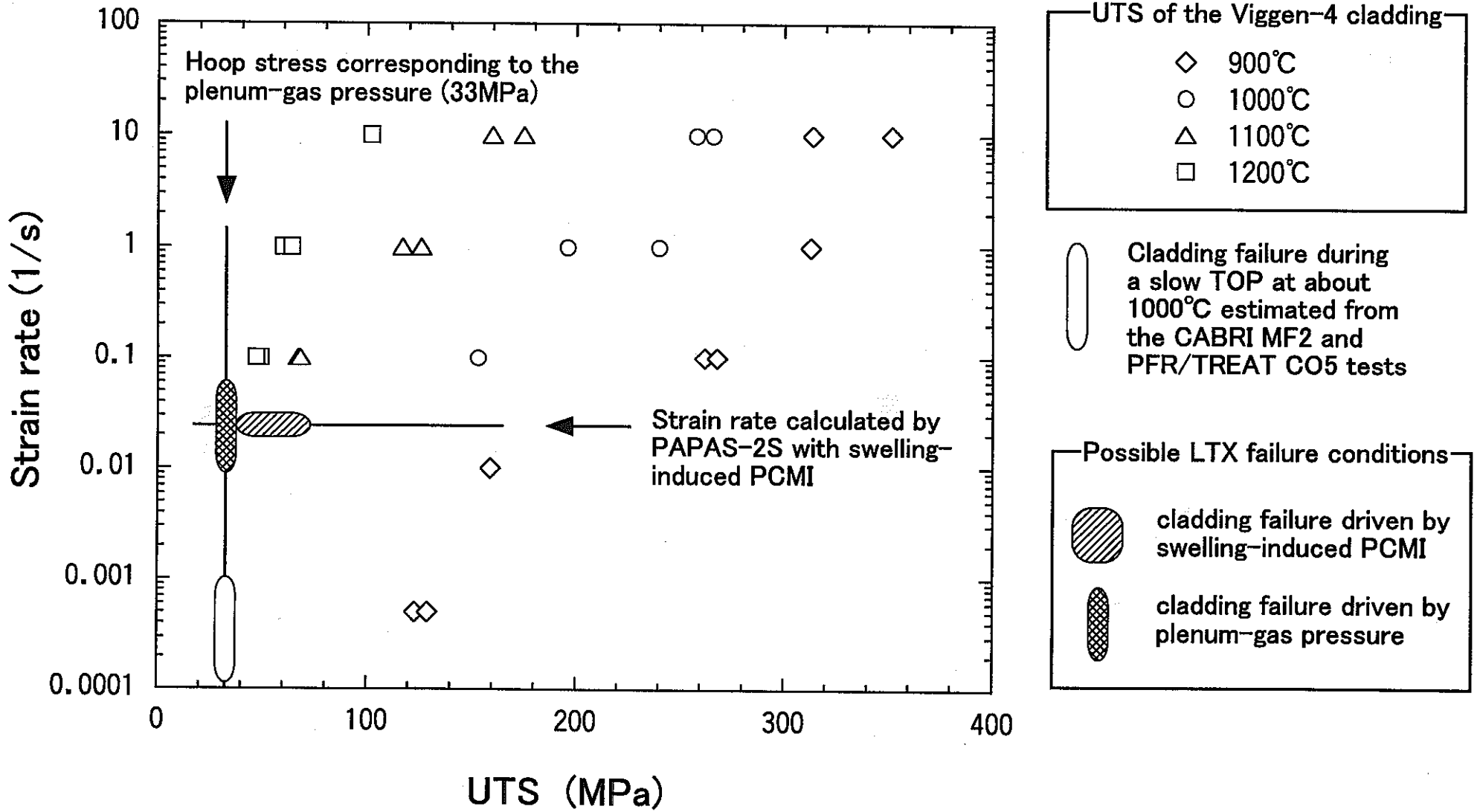

Figure28 UTS data from the Viggen-4 cladding and possible LTX failure conditions